Dish-STARS Commercialization

Final Report

June 2022

RF Zheng

DISCLAIMER

This report was prepared as an account of work sponsored by an agency of the United States Government. Neither the United States Government nor any agency thereof, nor Battelle Memorial Institute, nor any of their employees, makes **any warranty, express or implied, or assumes any legal liability or responsibility for the accuracy, completeness, or usefulness of any information, apparatus, product, or process disclosed, or represents that its use would not infringe privately owned rights**. Reference herein to any specific commercial product, process, or service by trade name, trademark, manufacturer, or otherwise does not necessarily constitute or imply its endorsement, recommendation, or favoring by the United States Government or any agency thereof, or Battelle Memorial Institute. The views and opinions of authors expressed herein do not necessarily state or reflect those of the United States Government or any agency thereof.

Dish-STARS Commercialization

RF Zheng

June 2022

Pacific Northwest National Laboratory
Richland, Washington 99352

Submitted To: U.S. Department of Energy, Solar Energy Technologies Office (SETO)
Project ID: TCF-16-12203
Field Work Proposal: 69121
Project Title: Solar Thermochemical Reaction system for Hydrogen Fuel Cell
Project Manager: Dr. Richard F. Zheng
                         Phone: 509-375-3604
                         richard.zheng@pnnl.gov
Submitting Official: Contracting Officer
Date Submitted: June 24, 2022
Recipient Organization: Pacific Northwest National Laboratory
                         P.O. Box 999
                         Richland, WA 99352
Project Period: September 28, 2016, through December 31, 2020
Report Period End Date: December 31, 2020
Reporting Term: Final Report
Signature:

Abstract

The goal of this project was to aggressively support the near-term commercialization of a new technology platform – based on the integration of solar concentrators and micro- and meso-channel process technology (MMPT) – that was evaluated and identified as a strong candidate for near-term commercialization at EERE's inaugural Lab-Corps program during early FY2016. Known as STARS, for Solar Thermochemical Advanced Reactor System, or Dish-STARS^{TM} when paired with parabolic dish concentrators, STARS is a promising energy-related technology developed at the Pacific Northwest National Laboratory (PNNL) that efficiently converts solar energy into chemical energy. Combined with economies through hardware mass production, the efficiency of Dish-STARS^{TM} provides a near-term opportunity for the production of renewable electricity, fuels, and chemicals.

The project supported the cooperative development of Dish-STARS^{TM} by PNNL and industry partners including California Gas Company (SoCalGas) and the startup company, STARS Technology Corporation (STC), which was founded by the PNNL Lab-Corps team that evaluated STARS on behalf of EERE. Under this project, the team advanced the Technology Readiness Level 6 (TRL 6) STARS reaction system, developed under the previous DOE SunShot project, to TRL 7 through on-sun testing in California by PNNL. The advances made in this project enabled STC to accelerate commercial development and initiate work towards a major technology demonstration in California for a hydrogen filling station application.

Acronyms and Abbreviations

BOM	bill of materials
CNC	computer numerical control
COGS	cost of goods sold
CSP	concentrating solar power
DOE	Department of Energy
DMLS	direct metal laser sintering
DNI	direct normal irradiance
FE	finite element
HHV	higher heating value
HTR	high temperature recuperation
IR	infrared
LCOE	levelized cost of electricity
LCOA	levelized cost of augment
MPV	minimum viable product
MMPT	meso- and microchannel processing technology
MMBTU	million British Thermal Units
PD3	PowerDish^{TM} III
PD4	PowerDish^{TM} IV
PD5	PowerDish^{TM} V
PDV	process development vehicle
PNNL	Pacific Northwest National Laboratory
PSA	pressure swing adsorption
S/C	steam to carbon ratio
SLM	selective laser melting
SMR	steam methane reforming
STARS^{TM}	Solar Thermal Advanced Reaction System^{TM}
TRL	technology readiness level
TDV	technology development vehicle
WGS	water gas shift

Contents

Figures

Tables

1.0   Program Goals and Objectives

This project aimed at the goal of supporting the near-term commercialization of a new technology platform – based on the integration of solar concentrators and micro- and meso-channel process technology (MMPT) – that was evaluated and identified as a strong candidate for near-term commercialization at EERE's inaugural Lab-Corps program during early FY2016. Known as STARS, for Solar Thermochemical Advanced Reactor System, or Dish-STARS^{TM} when paired with parabolic dish concentrators, STARS is a promising energy-related technology developed at the Pacific Northwest National Laboratory (PNNL) that efficiently converts solar energy into chemical energy. Combined with economies through hardware mass production, the efficiency of Dish-STARS^{TM} provides a near-term opportunity for the production of renewable electricity, fuels, and chemicals.

The project objectives were to:

- Support the cooperative development of Dish-STARS^{TM} by the DOE national laboratory and private partners, including the startup company, STARS Technology Corporation (STC), that was established by the PNNL Lab-Corps team that evaluated STARS on behalf of EERE.

- Provide important transition funding at the time that the previous DOE SunShot project, which has supported Dish-STARS^{TM} development from Technology Readiness Level 3 (TRL 3) to TRL 6, was scheduled to end.

- Help accelerate the commercial deployment of Dish-STARS^{TM}, enabling STC to aggressively accomplish, by the year 2020, the dual goals of ramping up to volume production (hundreds to thousands of Dish-STARS^{TM} units per year) – therefore achieving economics of hardware mass production – and groundbreaking for several major deployments by the year 2020.

- Support a near-term application identified through the Lab-Corps evaluations: The distributed production of hydrogen at a fuel cell vehicle refueling station in Palm Desert, California.

2.0 Accomplishments and Milestone Update

2.1 Synopsis of Accomplishments

The project team was able to meet all project milestones and success criteria during the project's period of performance. The project team developed technical specifications, designs, manufacturing plans and partners/vendors for the near-term commercial demonstration, specifically for applications of renewable hydrogen production for fuel cell vehicle filling stations in California. Technoeconomic assessments done under this project demonstrated that a Dish-STARS^{TM} system is projected to produce H_2 at a cost of \$2/kg when units are produced in volumes that achieve economies of hardware mass production.

2.2 Milestones

The program had multiple milestones associated with each task. All milestones were completed. Milestone M2-3 originally was planned to have the system tested on-sun for 300 hours. Actual test duration was reduced to 100 hours due to travel restrictions to the test site during COVID-19 pandemic.

Table 1. List of project milestones.

Milestone ID	Milestone Description	Responsible Organization	Planned Completion	Actual Completion
M1-1	Complete the technical specifications for the MVP version of Dish-STARS^{TM} for the fuel cell vehicle filling station application	PNNL	12/31/2017	3/31/2018
M2-1	Complete extended testing of TRL 6 Dish-STARS^{TM} system at Brawley	PNNL	6/30/2018	6/30/2018
M2-2	Initiate TRL 7 Dish-STARS^{TM} system tests at Brawley, CA	PNNL	10/31/2018	5/7/2019
M3-1	Complete the conceptual design for the MVP version of Dish-STARS^{TM} for the fuel cell filling station application	PNNL	10/31/2018	11/6/2018
M3-2	Complete the technoeconomic evaluation of the MVP version of Dish-STARS^{TM} for the fuel cell filling station application	STC	3/31/2019	12/31/2019
M2-3	Complete at least 300 on-sun hours of TRL 7 Dish-STARS^{TM} system tests at Brawley, CA	PNNL	10/31/2019	8/18/2020

2.3 Project Accomplishments by Task

2.3.1 WBS 1.0 Dish-STARS™ Integrated Commercial Design

2.3.1.1 Overview

This task leveraged the project team's prior evaluation of various parabolic dish concentrators, and their integration with the STARS reaction system, started during Phase 3 of the previous SunShot project. With input from STC, the project team had chosen the Infinia PowerDish III dish as the assumed baseline for future applications. Based on the previous work, the team expect that the Infinia PowerDish IV dish as well as dishes from various other developers/vendors will also be considered by STC for further development and commercialization of Dish-STARS™ (though not as part of this project).

A thermochemical process for hydrogen production from natural gas, based on PNNL's STARS technology platform, was specified after extensive Aspen Plus and CHEMCAD process modeling and flowsheet development. Specifically, the process flowsheet was finalized for an onsite plant with 125 kg-H_2/day output at a hydrogen filling station for fuel cell electric vehicles. This process was intended as the minimum viable product (MVP) version under development by this project and was leveraged to provide flowsheet guidance for further manufacturing development under the concurrent RAPID JumpStart project. As part of the front-end loading stage 1 (FEL-1) activity for a SoCalGas led commercial demonstration project to be proposed in California, this project team PNNL provided the current MVP Dish-STARS™ specifications as its recommendation for further conceptual development.

2.3.1.2 Initial MVP Design Specifications

During the first six months of the project, a STARS process flowsheet using hydrogen membrane separation and syngas recompression was initially evaluated for the MVP design. The high-level block diagram of this process is shown in Figure 1. The major equipment and functions are tabulated in Table 2. The parabolic solar concentrator dish was the Infinia PowerDish III, assuming each SMR reactor train would be paired with one dish. The sensible and latent heat from syngas and hydrogen product streams were recovered by recuperative heat exchangers to generate steam. The reformate compressor slightly compresses the reformate stream to raise its vapor dome so that more heat can be recovered without a pinch problem from hot stream phase change, as evident in the simulated vaporizer temperature profiles shown in Figure 2. An additional trim heat exchanger installed around dish receiver will capture spillage solar flux to bring vapor fraction of the steam to close unity. Recovery of 95% hydrogen from reformate was specified for a palladium-metal microchannel membrane unit.

Figure 1. Block diagram of the STARS section of the initial MVP design.

Figure 2. Temperature profiles of the low temperature vaporizer (LTV) from Aspen Plus simulation showing no double pinch.

Table 2. Major equipment list of the initial MVP design on-sun section excluding the parabolic dish.
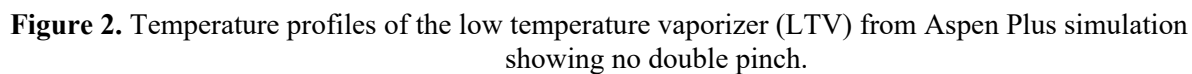
Name	Streams	Function	Duty	Equipment Type
Feed Stream mixer	Feed water, feed methane	Mixing liquid water and methane gas	~0	Nozzle expansion
LT Vaporizer	Feed mixture, compressed reformate, H_2	Vaporize water to 2/3 vapor fraction at 168°C	4.2 kWt	304 SS 3-stream microchannel heat exchanger
HT Vaporizer	Feed mixture, reformate, H_2	Bring feed vapor fraction to 0.91 at 176°C	1.8 kWt	304 SS 3-stream heat microchannel exchanger

Reformate Compressor	H$_2$-lean reformate	Slightly compress reformate to raise vapor dome (~24% pressure increase)	0.15 kWe	DC motor driven centrifugal blower
H$_2$ Membrane Separator	Reformate	Recover 95% H$_2$ from reformate	~0	Pd metal microchannel membrane unit
Spillage Heater	Steam methane mixture	Heat feed mixture to close vapor fraction of 1 using insolation spillage	0.6 kWt	304 SS microchannel heat exchanger
HT Recuperator	Reformate, feed mixture	Superheat feed mixture using hot reformate	4.0 kWt	Inconel microchannel heat exchanger
SMR Reactor	Feed mixture	Convert methane steam mixture to syngas using concentrated solar energy	9.3 kWt	Haynes 230 microchannel reactor

The SMR unit in the above design was specified as nominally the same size as the TRL 6 STARS system first developed under the SunShot project and improved and tested further under this project. The performance of this TRL 6 system paired with a PowerDish III parabolic dish solar concentrator is listed in Table 3 based on actual tests.

Table 3. An example of TRL 6 Dish-STARS reactor performance.

Parameters	Value	
Heat Duty, kW	8.22	
SMR Energy Input	Solar, Infinia PowerDish III	
Inlet Temperature, °C	666	
Outlet Temperature, °C	718	
Mean Temperature at Channel Exits	819	
Inlet Pressure, bar	7.82	
Pressure Drop, bar	0.14	
Mass Flow Rate, kg/h	9.292	
Feed Methane Rate, mol/s	0.046	
Feed Steam Rate, mol/s	0.102	
Steam to Carbon Ratio	2.2	
Hydrogen Product Rate, kg/h	0.870	
Stream Composition, mole fraction	In	Out
H$_2$	0.000	0.546
CH$_4$	0.313	0.045
CO	0.000	0.113
CO$_2$	0.000	0.052
H$_2$O	0.687	0.244

2.3.1.3   Refined MVP Design

During the second half of year 2018, the project team refined the MVP design based on input from STC and SoCalGas on the specific requirements for a potential first near-term commercial demonstration in California. The updated MVP STARS was envisioned to be a hybrid steam methane reforming (SMR) plant having two groups of SMR units running on either concentrated solar or grid electrical energy as input for the endothermic reaction. The size of each SMR unit is nominally the same as the TRL 6 STAR

system (Table 3). The hydrogen separation and purification were done with a commercial pressure swing adsorption process instead of palladium hydrogen membranes. The total hydrogen production capacity was 125 kg/day. The key specifications of the SMR plant are summarized in Table 4.

Table 4. Key specifications of MVP STARS process.

Parameters	Value
Hydrogen production rate, kg/day (peak hour)	125
SMR methane conversion	90% at 800°C, 5 bar, and 3:1 steam/carbon ratio
WGS conversion	90% at 225°C inlet
Number of solar SMR reactors	2
Parabolic solar concentrator	Infinia PowerDish III
Number of electric heating SMR reactors	3
Hydrogen separation	Pressure swing adsorption
PSA hydrogen recovery	90%
Steam generation	PSA tail gas combustion
Combustor temperature	550°C
Heat exchanger minimum approach, °C	15

The MVP STARS process was simulated using an Aspen Plus model. The main flowsheet is shown in Figure 3. The stream properties are summarized in Table 5. The specifications of the process heat exchangers are listed in Table 9.

The SMR plant was divided into a "sSMR" section powered by concentrated solar at a total heat duty of 17.8 kW and an "eSMR" section powered by induction electrical heating at a total heat duty of 26.8 kW. The solar section consisted of two SMR reactors. The electrical SMR section consisted of three SMR reactors. All SMR reactors were envisioned to be the same size as the TRL 6 reactor and operates at close to 9 kW heat duty. Each SMR section was served by a separate train of high temperature recuperator, low temperature recuperator, steam generator, water gas shift reactor, and vapor liquid separator.

The combined syngas products were fed to a PSA unit that produce fuel cell grade hydrogen at 90% recovery. A portion of the PSA tail gas was used as fuel in the combustion vaporizer for steam generation. A three-stage combustor/vaporizer design was used to keep combustion temperature under 550°C, allowing low-cost stainless steel as the material of construction. The remaining tail gas was flared. In the current design a separate steam generator and a WGS reactor was specified for each of the SMR sections. However, it was expected that they may be combined into a single steam generator and a single WGS reactor depending on equipment sizing during the conceptual design stage.
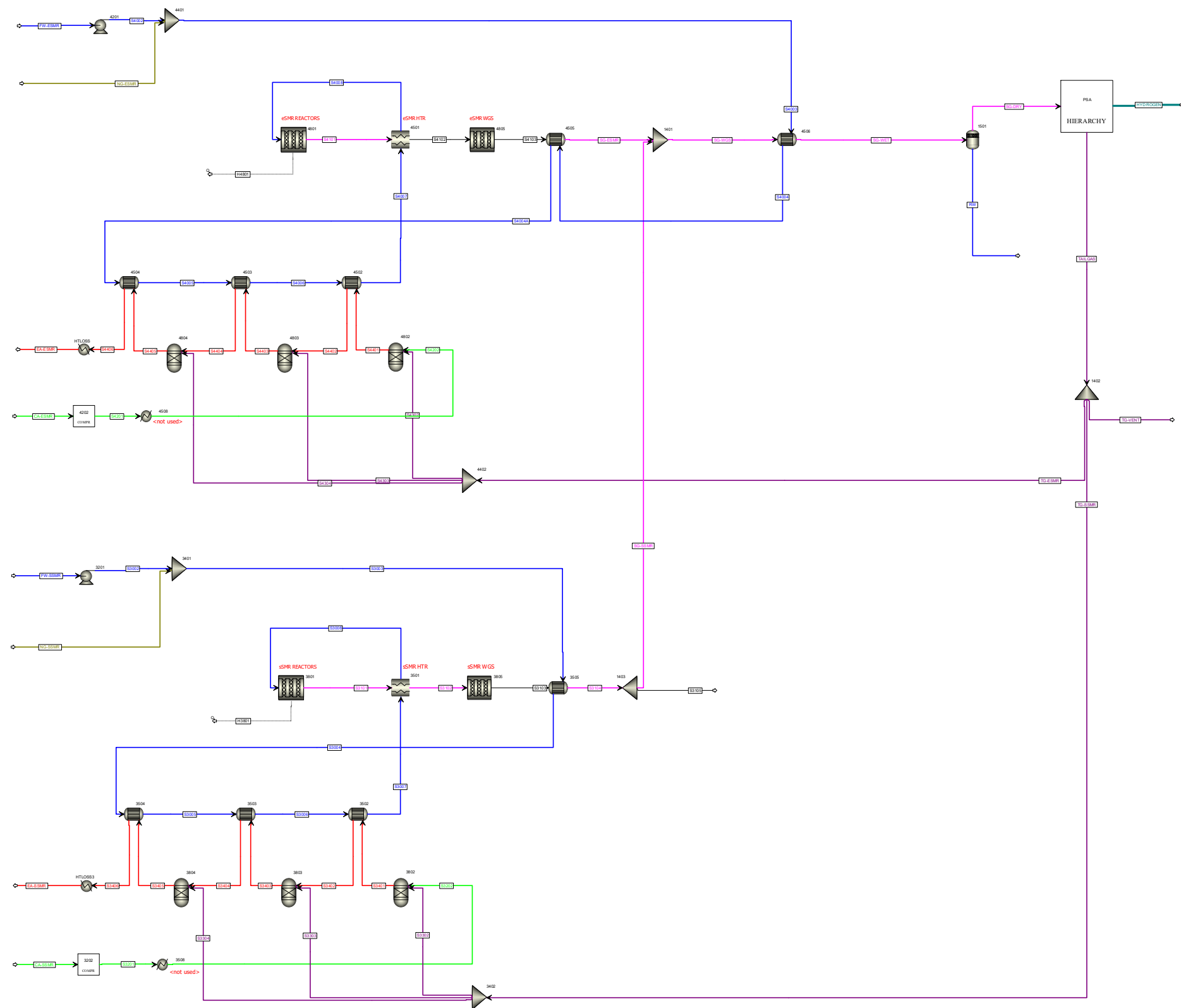
Figure 3. Aspen Plus process flowsheet of the MVP STARS system.

Table 5. MVP STARS process stream table.

Stream Name	Units	CA-ESMR	CA-SSMR	EA-ESMR	EA-SSMR	FW-ESMR	FW-SSMR	HYDROGEN	NG-ESMR	NG-SSMR	RW	S3002	S3003	S3004	S3005	S3006	S3007
From				HTLOSS	HTLOSS3			PSA			1501	3201	3401	3505	3504	3503	3502
To		4202	3202			4201	3201		4401	3401		3401	3505	3504	3503	3502	3501
Phase		Vapor	Vapor	Vapor	Vapor	Liquid	Liquid	Vapor	Vapor	Vapor	Liquid	Liquid					
Temperature	C	22.0	22.0	60.0	60.0	25.0	25.0	60.0	25.0	25.0	60.0	25.0	24.0	125.9	134.5	139.0	141.2
Pressure	bar	1.013	1.013	1.010	1.010	5.000	5.000	4.500	5.000	5.000	4.500	5.000	5.000	5.000	5.000	5.000	5.000
Molar Vapor Fraction		1	1	1	1	0	0	1	1	1	0	0	0.252	0.478	0.655	0.838	0.989
Mass Vapor Fraction		1	1	1	1	0	0	1	1	1	0	0	0.230	0.464	0.645	0.834	0.989
Molar Enthalpy	J/kmol	-9.441E+04	-9.441E+04	-1.183E+08	-1.163E+08	-2.858E+08	-2.858E+08	1.015E+06	-7.460E+07	-7.460E+07	-2.831E+08	-2.858E+08	-2.330E+08	-2.173E+08	-2.099E+08	-2.025E+08	-1.966E+08
Mass Enthalpy	J/kg	-3272.26	-3.272E+03	-3.941E+06	-3.878E+06	-1.586E+07	-1.586E+07	5.037E+05	-4.650E+06	-4.650E+06	-1.572E+07	-1.586E+07	-1.330E+07	-1.240E+07	-1.198E+07	-1.156E+07	-1.122E+07
Molar Entropy	J/kmol-K	3956.40	3.956E+03	6.373E+03	6.460E+03	-1.632E+05	-1.632E+05	-9.195E+03	-9.408E+04	-9.408E+04	-1.548E+05	-1.632E+05	-1.459E+05	-1.026E+05	-8.431E+04	-6.632E+04	-5.190E+04
Mass Entropy	J/kg-K	137.13	1.371E+02	2.124E+02	2.154E+02	-9.059E+03	-9.059E+03	-4.561E+03	-5.864E+03	-5.864E+03	-8.595E+03	-9.059E+03	-8.327E+03	-5.857E+03	-4.812E+03	-3.785E+03	-2.962E+03
Molar Density	kmol/m^3	4.130E-02	4.130E-02	3.652E-02	3.652E-02	5.536E+01	5.536E+01	1.621E-01	2.034E-01	2.034E-01	5.458E+01	5.536E+01	8.031E-01	3.185E-01	2.291E-01	1.775E-01	1.499E-01
Mass Density	kg/cm^3	1.191E+00	1.191E+00	1.096E+00	1.095E+00	9.972E+02	9.972E+02	3.268E-01	3.264E+00	3.264E+00	9.833E+02	9.972E+02	1.407E+01	5.581E+00	4.014E+00	3.111E+00	2.627E+00
Enthalpy Flow	W	-2.123E+01	-1.555E+01	-3.670E+04	-2.626E+04	-1.193E+05	-7.927E+04	7.392E+02	-1.038E+04	-6.898E+03	-7.199E+04	-7.927E+04	-8.617E+04	-8.036E+04	-7.762E+04	-7.490E+04	-7.269E+04
Average MW		28.85	28.85	30.01	29.99	18.02	18.02	2.02	16.04	16.04	18.02	18.02	17.52	17.52	17.52	17.52	17.52
Mole Flows	kmol/hr	0.8097	0.5929	1.1172	0.8129	1.5025	0.9986	2.6210	0.5008	0.3329	0.9153	0.9986	1.3314	1.3314	1.3314	1.3314	1.3314
Mole Fractions																	
H_2		0.0000	0.0000	0.0000	0.0000	0.0000	0.0000	1.0000	0.0000	0.0000	0.0000	0.0000	0.0000	0.0000	0.0000	0.0000	0.0000
N_2		0.7900	0.7900	0.5726	0.5761	0.0000	0.0000	0.0000	0.0000	0.0000	0.0000	0.0000	0.0000	0.0000	0.0000	0.0000	0.0000
O_2		0.2100	0.2100	0.0636	0.0660	0.0000	0.0000	0.0000	0.0000	0.0000	0.0000	0.0000	0.0000	0.0000	0.0000	0.0000	0.0000
CO_2		0.0000	0.0000	0.2069	0.2035	0.0000	0.0000	0.0000	0.0000	0.0000	0.0000	0.0000	0.0000	0.0000	0.0000	0.0000	0.0000
H_2S		0.0000	0.0000	0.0000	0.0000	0.0000	0.0000	0.0000	0.0000	0.0000	0.0000	0.0000	0.0000	0.0000	0.0000	0.0000	0.0000
CH_4		0.0000	0.0000	0.0000	0.0000	0.0000	0.0000	0.0000	1.0000	1.0000	0.0000	0.0000	0.2500	0.2500	0.2500	0.2500	0.2500
H_2O		0.0000	0.0000	0.1569	0.1543	1.0000	1.0000	0.0000	0.0000	0.0000	1.0000	1.0000	0.7500	0.7500	0.7500	0.7500	0.7500
CO		0.0000	0.0000	0.0000	0.0000	0.0000	0.0000	0.0000	0.0000	0.0000	0.0000	0.0000	0.0000	0.0000	0.0000	0.0000	0.0000
Mass Flows	kg/hr	23.361	17.104	33.525	24.379	27.069	17.990	5.284	8.035	5.340	16.490	17.990	23.330	23.330	23.330	23.330	23.330
Mass Fractions																	
H_2		0.0000	0.0000	0.0000	0.0000	0.0000	0.0000	1.0000	0.0000	0.0000	0.0000	0.0000	0.0000	0.0000	0.0000	0.0000	0.0000
N_2		0.7671	0.7671	0.5345	0.5382	0.0000	0.0000	0.0000	0.0000	0.0000	0.0000	0.0000	0.0000	0.0000	0.0000	0.0000	0.0000
O_2		0.2329	0.2329	0.0678	0.0705	0.0000	0.0000	0.0000	0.0000	0.0000	0.0000	0.0000	0.0000	0.0000	0.0000	0.0000	0.0000
CO_2		0.0000	0.0000	0.3034	0.2986	0.0000	0.0000	0.0000	0.0000	0.0000	0.0000	0.0000	0.0000	0.0000	0.0000	0.0000	0.0000
H_2S		0.0000	0.0000	0.0000	0.0000	0.0000	0.0000	0.0000	0.0000	0.0000	0.0000	0.0000	0.0000	0.0000	0.0000	0.0000	0.0000
CH_4		0.0000	0.0000	0.0000	0.0000	0.0000	0.0000	0.0000	1.0000	1.0000	0.0000	0.0000	0.2289	0.2289	0.2289	0.2289	0.2289
H_2O		0.0000	0.0000	0.0942	0.0927	1.0000	1.0000	0.0000	0.0000	0.0000	1.0000	1.0000	0.7711	0.7711	0.7711	0.7711	0.7711
CO		0.0000	0.0000	0.0000	0.0000	0.0000	0.0000	0.0000	0.0000	0.0000	0.0000	0.0000	0.0000	0.0000	0.0000	0.0000	0.0000
Volume Flow	m^3/hr	19.607	14.356	30.594	22.262	0.027	0.018	16.168	2.462	1.636	0.017	0.018	1.658	4.180	5.812	7.499	8.881

Table 6. MVP STARS process stream table (continued).

Stream Name	Units	S3008	S3101	S3102	S3103	S3104	S3201	S3202	S3302	S3303	S3304	S3401	S3402	S3403	S3404	S3405	S3406
From		3501	3801	3501	3805	3505	3202	3508	3402	3402	3402	3802	3502	3803	3503	3804	3504
To		3801	3501	3805	3505	1403	3508	3802	3802	3803	3804	3502	3803	3503	3804	3504	HTLOSS3
Phase		Vapor	Vapor	Vapor	Vapor		Vapor	Vapor				Vapor	Vapor	Vapor	Vapor	Vapor	Vapor
Temperature	C	773.4	785.0	225.0	313.6	90.0	26.4	26.4	60.0	60.0	60.0	549.9	189.0	571.9	184.5	522.4	175.9
Pressure	bar	4.950	4.850	4.750	4.650	4.650	1.051	1.051	4.500	4.500	4.500	1.041	1.041	1.031	1.031	1.021	1.021
Molar Vapor Fraction		1	1	1	1	0.916	1	1	0.906	0.906	0.906	1	1	1	1	1	1
Mass Vapor Fraction		1	1	1	1	0.874	1	1	0.940	0.940	0.940	1	1	1	1	1	1
Molar Enthalpy	J/kmol	-1.686E+08	-8.308E+07	-1.024E+08	-1.024E+08	-1.132E+08	3.304E+04	3.304E+04	-2.480E+08	-2.480E+08	-2.480E+08	-3.404E+07	-4.584E+07	-6.925E+07	-8.247E+07	-1.004E+08	-1.125E+08
Mass Enthalpy	J/kg	-9.622E+06	-6.875E+06	-8.470E+06	-8.470E+06	-9.366E+06	1.145E+03	1.145E+03	-8.787E+06	-8.787E+06	-8.787E+06	-1.160E+06	-1.562E+06	-2.332E+06	-2.777E+06	-3.349E+06	-3.753E+06
Molar Entropy	J/kmol-K	-1.141E+04	3.222E+04	6.654E+03	8.497E+03	-1.669E+04	4.084E+03	4.084E+03	-1.284E+04	-1.284E+04	-1.284E+04	3.700E+04	1.820E+04	3.831E+04	1.750E+04	3.596E+04	1.609E+04
Mass Entropy	J/kg-K	-6.514E+02	2.667E+03	5.506E+02	7.031E+02	-1.381E+03	1.416E+02	1.416E+02	-4.549E+02	-4.549E+02	-4.549E+02	1.261E+03	6.203E+02	1.290E+03	5.892E+02	1.199E+03	5.364E+02
Molar Density	kmol/m³	5.689E-02	5.508E-02	1.148E-01	9.527E-02	1.683E-01	4.219E-02	4.219E-02	1.805E-01	1.805E-01	1.805E-01	1.520E-02	2.708E-02	1.466E-02	2.709E-02	1.543E-02	2.735E-02
Mass Density	kg/cm³	9.968E-01	6.657E-01	1.387E+00	1.151E+00	2.034E+00	1.217E+00	1.217E+00	5.092E+00	5.092E+00	5.092E+00	4.461E-01	7.946E-01	4.355E-01	8.044E-01	4.626E-01	8.201E-01
Enthalpy Flow	W	-6.236E+04	-4.455E+04	-5.489E+04	-5.489E+04	-6.070E+04	5.441E+00	5.441E+00	-6.356E+03	-5.735E+03	-5.664E+03	-6.351E+03	-8.553E+03	-1.429E+04	-1.702E+04	-2.268E+04	-2.541E+04
Average MW		17.52	12.08	12.08	12.08	12.08	28.85	28.85	28.22	28.22	28.22	29.34	29.34	29.70	29.70	29.99	29.99
Mole Flows	kmol/hr	1.3314	1.9305	1.9305	1.9305	1.9305	0.5929	0.5929	0.0923	0.0833	0.0822	0.6716	0.6716	0.7427	0.7427	0.8129	0.8129
Mole Fractions																	
H_2		0.0000	0.5302	0.5302	0.6049	0.6049	0.0000	0.0000	0.2242	0.2242	0.2242	0.0000	0.0000	0.0000	0.0000	0.0000	0.0000
N_2		0.0000	0.0000	0.0000	0.0000	0.0000	0.7900	0.7900	0.0000	0.0000	0.0000	0.6973	0.6973	0.6306	0.6306	0.5761	0.5761
O_2		0.0000	0.0000	0.0000	0.0000	0.0000	0.2100	0.2100	0.0000	0.0000	0.0000	0.1476	0.1476	0.1027	0.1027	0.0660	0.0660
CO_2		0.0000	0.0647	0.0647	0.1394	0.1394	0.0000	0.0000	0.5092	0.5092	0.5092	0.0882	0.0882	0.1517	0.1517	0.2035	0.2035
H_2S		0.0000	0.0000	0.0000	0.0000	0.0000	0.0000	0.0000	0.0000	0.0000	0.0000	0.0000	0.0000	0.0000	0.0000	0.0000	0.0000
CH_4		0.2500	0.0173	0.0173	0.0173	0.0173	0.0000	0.0000	0.0642	0.0642	0.0642	0.0000	0.0000	0.0000	0.0000	0.0000	0.0000
H_2O		0.7500	0.2974	0.2974	0.2227	0.2227	0.0000	0.0000	0.1340	0.1340	0.1340	0.0669	0.0669	0.1150	0.1150	0.1543	0.1543
CO		0.0000	0.0904	0.0904	0.0157	0.0157	0.0000	0.0000	0.0684	0.0684	0.0684	0.0000	0.0000	0.0000	0.0000	0.0000	0.0000
Mass Flows	kg/hr	23.330	23.330	23.330	23.330	23.330	17.104	17.104	2.604	2.350	2.321	19.709	19.709	22.058	22.058	24.379	24.379
Mass Fractions																	
H_2		0.0000	0.0884	0.0884	0.1009	0.1009	0.0000	0.0000	0.0160	0.0160	0.0160	0.0000	0.0000	0.0000	0.0000	0.0000	0.0000
N_2		0.0000	0.0000	0.0000	0.0000	0.0000	0.7671	0.7671	0.0000	0.0000	0.0000	0.6657	0.6657	0.5948	0.5948	0.5382	0.5382
O_2		0.0000	0.0000	0.0000	0.0000	0.0000	0.2329	0.2329	0.0000	0.0000	0.0000	0.1610	0.1610	0.1106	0.1106	0.0705	0.0705
CO_2		0.0000	0.2357	0.2357	0.5078	0.5078	0.0000	0.0000	0.7940	0.7940	0.7940	0.1323	0.1323	0.2248	0.2248	0.2986	0.2986
H_2S		0.0000	0.0000	0.0000	0.0000	0.0000	0.0000	0.0000	0.0000	0.0000	0.0000	0.0000	0.0000	0.0000	0.0000	0.0000	0.0000
CH_4		0.2289	0.0229	0.0229	0.0229	0.0229	0.0000	0.0000	0.0365	0.0365	0.0365	0.0000	0.0000	0.0000	0.0000	0.0000	0.0000
H_2O		0.7711	0.4433	0.4433	0.3319	0.3319	0.0000	0.0000	0.0856	0.0856	0.0856	0.0411	0.0411	0.0698	0.0698	0.0927	0.0927
CO		0.0000	0.2096	0.2096	0.0364	0.0364	0.0000	0.0000	0.0679	0.0679	0.0679	0.0000	0.0000	0.0000	0.0000	0.0000	0.0000
Volume Flow	m³/hr	23.404	35.048	16.823	20.264	11.472	14.051	14.051	0.511	0.461	0.456	44.183	24.803	50.650	27.422	52.696	29.727

Table 7. MVP STARS process stream table (continued).

Stream Name	Units	S4002	S4003	S4004	S4004A	S4005	S4006	S4007	S4008	S4101	S4102	S4103	S4201	S4202	S4302	S4303	S4304
From		4201	4401	4506	4505	4504	4503	4502	4501	4801	4501	4805	4202	4508	4402	4402	4402
To		4401	4506	4505	4504	4503	4502	4501	4801	4501	4805	4505	4508	4802	4802	4803	4804
Phase		Liquid								Vapor	Vapor	Vapor	Vapor	Vapor	Vapor		
Temperature	C	25.0	24.0	94.2	128.2	135.6	139.2	141.2	773.4	785.0	225.0	308.3	26.4	26.4	60.0	60.0	60.0
Pressure	bar	5.000	5.000	5.000	5.000	5.000	5.000	5.000	4.950	4.850	4.750	4.650	1.051	1.051	4.500	4.500	4.500
Molar Vapor Fraction		0	0.252	0.299	0.513	0.691	0.852	0.989	1	1	1	1	1	1	0.906	0.906	0.906
Mass Vapor Fraction		0	0.230	0.280	0.499	0.682	0.848	0.989	1	1	1	1	1	1	0.940	0.940	0.940
Molar Enthalpy	J/kmol	-2.858E+08	-2.330E+08	-2.264E+08	-2.158E+08	-2.084E+08	-2.020E+08	-1.966E+08	-1.686E+08	-8.307E+07	-1.023E+08	-1.024E+08	3.304E+04	3.304E+04	-2.480E+08	-2.480E+08	-2.480E+08
Mass Enthalpy	J/kg	-1.586E+07	-1.330E+07	-1.292E+07	-1.232E+07	-1.189E+07	-1.153E+07	-1.122E+07	-9.622E+06	-6.874E+06	-8.469E+06	-8.470E+06	1.145E+03	1.145E+03	-8.787E+06	-8.787E+06	-8.787E+06
Molar Entropy	J/kmol-K	-1.632E+05	-1.459E+05	-1.263E+05	-9.893E+04	-8.071E+04	-6.498E+04	-5.190E+04	-1.142E+04	3.223E+04	6.658E+03	8.469E+03	4.084E+03	4.084E+03	-1.284E+04	-1.284E+04	-1.284E+04
Mass Entropy	J/kg-K	-9.059E+03	-8.327E+03	-7.208E+03	-5.646E+03	-4.606E+03	-3.709E+03	-2.962E+03	-6.515E+02	2.667E+03	5.509E+02	7.008E+02	1.416E+02	1.416E+02	-4.549E+02	-4.549E+02	-4.549E+02
Molar Density	kmol/m^3	5.536E+01	8.031E-01	5.472E-01	2.960E-01	2.167E-01	1.746E-01	1.499E-01	5.689E-02	5.508E-02	1.148E-01	9.614E-02	4.219E-02	4.219E-02	1.805E-01	1.805E-01	1.805E-01
Mass Density	kg/cm^3	9.972E+02	1.407E+01	9.588E+00	5.186E+00	3.796E+00	3.059E+00	2.627E+00	9.968E-01	6.656E-01	1.387E+00	1.162E+00	1.217E+00	1.217E+00	5.092E+00	5.092E+00	5.092E+00
Enthalpy Flow	W	-1.193E+05	-1.297E+05	-1.260E+05	-1.201E+05	-1.160E+05	-1.124E+05	-1.094E+05	-9.383E+04	-6.703E+04	-8.259E+04	-8.259E+04	7.431E+00	7.431E+00	-8.683E+03	-7.566E+03	-8.559E+03
Average MW		18.02	17.52	17.52	17.52	17.52	17.52	17.52	17.52	12.08	12.08	12.08	28.85	28.85	28.22	28.22	28.22
Mole Flows	kmol/hr	1.5025	2.0034	2.0034	2.0034	2.0034	2.0034	2.0034	2.0034	2.9049	2.9049	2.9049	0.8097	0.8097	0.1261	0.1099	0.1243
Mole Fractions																	
H$_2$		0.0000	0.0000	0.0000	0.0000	0.0000	0.0000	0.0000	0.0000	0.5302	0.5302	0.6005	0.0000	0.0000	0.2242	0.2242	0.2242
N$_2$		0.0000	0.0000	0.0000	0.0000	0.0000	0.0000	0.0000	0.0000	0.0000	0.0000	0.0000	0.7900	0.7900	0.0000	0.0000	0.0000
O$_2$		0.0000	0.0000	0.0000	0.0000	0.0000	0.0000	0.0000	0.0000	0.0000	0.0000	0.0000	0.2100	0.2100	0.0000	0.0000	0.0000
CO$_2$		0.0000	0.0000	0.0000	0.0000	0.0000	0.0000	0.0000	0.0000	0.0647	0.0647	0.1350	0.0000	0.0000	0.5092	0.5092	0.5092
H$_2$S		0.0000	0.0000	0.0000	0.0000	0.0000	0.0000	0.0000	0.0000	0.0000	0.0000	0.0000	0.0000	0.0000	0.0000	0.0000	0.0000
CH$_4$		0.0000	0.2500	0.2500	0.2500	0.2500	0.2500	0.2500	0.2500	0.0173	0.0173	0.0173	0.0000	0.0000	0.0642	0.0642	0.0642
H$_2$O		1.0000	0.7500	0.7500	0.7500	0.7500	0.7500	0.7500	0.7500	0.2974	0.2974	0.2271	0.0000	0.0000	0.1340	0.1340	0.1340
CO		0.0000	0.0000	0.0000	0.0000	0.0000	0.0000	0.0000	0.0000	0.0905	0.0905	0.0201	0.0000	0.0000	0.0684	0.0684	0.0684
Mass Flows	kg/hr	27.069	35.104	35.104	35.104	35.104	35.104	35.104	35.104	35.104	35.104	35.104	23.361	23.361	3.557	3.100	3.507
Mass Fractions																	
H$_2$		0.0000	0.0000	0.0000	0.0000	0.0000	0.0000	0.0000	0.0000	0.0884	0.0884	0.1002	0.0000	0.0000	0.0160	0.0160	0.0160
N$_2$		0.0000	0.0000	0.0000	0.0000	0.0000	0.0000	0.0000	0.0000	0.0000	0.0000	0.0000	0.7671	0.7671	0.0000	0.0000	0.0000
O$_2$		0.0000	0.0000	0.0000	0.0000	0.0000	0.0000	0.0000	0.0000	0.0000	0.0000	0.0000	0.2329	0.2329	0.0000	0.0000	0.0000
CO$_2$		0.0000	0.0000	0.0000	0.0000	0.0000	0.0000	0.0000	0.0000	0.2357	0.2357	0.4918	0.0000	0.0000	0.7940	0.7940	0.7940
H$_2$S		0.0000	0.0000	0.0000	0.0000	0.0000	0.0000	0.0000	0.0000	0.0000	0.0000	0.0000	0.0000	0.0000	0.0000	0.0000	0.0000
CH$_4$		0.0000	0.2289	0.2289	0.2289	0.2289	0.2289	0.2289	0.2289	0.0229	0.0229	0.0229	0.0000	0.0000	0.0365	0.0365	0.0365
H$_2$O		1.0000	0.7711	0.7711	0.7711	0.7711	0.7711	0.7711	0.7711	0.4433	0.4433	0.3385	0.0000	0.0000	0.0856	0.0856	0.0856
CO		0.0000	0.0000	0.0000	0.0000	0.0000	0.0000	0.0000	0.0000	0.2097	0.2097	0.0467	0.0000	0.0000	0.0679	0.0679	0.0679
Volume Flow	m^3/hr	0.027	2.495	3.661	6.769	9.247	11.475	13.363	35.215	52.738	25.313	30.216	19.191	19.191	0.699	0.609	0.689

Table 8. MVP STARS process stream table (continued).

Stream Name	Units	S4401	S4402	S4403	S4404	S4405	S4406	SG-DRY	SG-ESMR	SG-SSMR	SG-WET	SG-WGS	TAILGAS	TG-ESMR	TG-SSMR	TG-VENT
From		4802	4502	4803	4503	4804	4504	1501	4505	1403	4506	1401	PSA	1402	1402	1402
To		4502	4803	4503	4804	4504	HTLOSS	PSA	1401	1401	1501	4506	1402	4402	3402	
Phase		Vapor	Vapor	Vapor	Vapor	Vapor	Vapor	Vapor								
Temperature	C	550.0	189.2	561.3	185.6	554.5	178.2	60.0	100.0	90.0	87.8	96.5	60.0	60.0	60.0	60.0
Pressure	bar	1.041	1.041	1.031	1.031	1.021	1.021	4.500	4.650	4.650	4.650	4.650	4.500	4.500	4.500	4.500
Molar Vapor Fraction		1	1	1	1	1	1	1	0.989	0.916	0.900	0.959	0.906	0.906	0.906	0.906
Mass Vapor Fraction		1	1	1	1	1	1	1	0.983	0.874	0.851	0.939	0.940	0.940	0.940	0.940
Molar Enthalpy	J/kmol	-3.404E+07	-4.584E+07	-6.853E+07	-8.132E+07	-1.012E+08	-1.144E+08	-8.016E+07	-1.097E+08	-1.132E+08	-1.138E+08	-1.111E+08	-2.480E+08	-2.480E+08	-2.480E+08	-2.480E+08
Mass Enthalpy	J/kg	-1.160E+06	-1.562E+06	-2.308E+06	-2.739E+06	-3.372E+06	-3.813E+06	-7.492E+06	-9.076E+06	-9.366E+06	-9.417E+06	-9.192E+06	-8.787E+06	-8.787E+06	-8.787E+06	-8.787E+06
Molar Entropy	J/kmol-K	3.700E+04	1.822E+04	3.786E+04	1.760E+04	3.739E+04	1.619E+04	-3.318E+03	-7.339E+03	-1.669E+04	-1.851E+04	-1.104E+04	-1.284E+04	-1.284E+04	-1.284E+04	-1.284E+04
Mass Entropy	J/kg-K	1.261E+03	6.208E+02	1.275E+03	5.929E+02	1.246E+03	5.394E+02	-3.101E+02	-6.073E+02	-1.381E+03	-1.531E+03	-9.136E+02	-4.549E+02	-4.549E+02	-4.549E+02	-4.549E+02
Molar Density	kmol/m³	1.520E-02	2.707E-02	1.485E-02	2.702E-02	1.483E-02	2.721E-02	1.623E-01	1.519E-01	1.683E-01	1.722E-01	1.580E-01	1.805E-01	1.805E-01	1.805E-01	1.805E-01
Mass Density	kg/cm³	4.460E-01	7.942E-01	4.409E-01	8.022E-01	4.450E-01	8.164E-01	1.737E+00	1.835E+00	2.034E+00	2.081E+00	1.909E+00	5.092E+00	5.092E+00	5.092E+00	5.092E+00
Enthalpy Flow	W	-8.675E+03	-1.168E+04	-1.925E+04	-2.284E+04	-3.140E+04	-3.551E+04	-8.729E+04	-8.850E+04	-6.070E+04	-1.529E+05	-1.492E+05	-8.948E+04	-2.481E+04	-1.776E+04	-4.691E+04
Average MW		29.34	29.34	29.69	29.69	30.01	30.01	10.70	12.08	12.08	12.08	12.08	28.22	28.22	28.22	28.22
Mole Flows	kmol/hr	0.9174	0.9174	1.0111	1.0111	1.1172	1.1172	3.9200	2.9049	1.9305	4.8353	4.8353	1.2991	0.3602	0.2578	0.6811
Mole Fractions																
H₂		0.0000	0.0000	0.0000	0.0000	0.0000	0.0000	0.7429	0.6005	0.6049	0.6023	0.6023	0.2242	0.2242	0.2242	0.2242
N₂		0.6973	0.6973	0.6326	0.6326	0.5726	0.5726	0.0000	0.0000	0.0000	0.0000	0.0000	0.0000	0.0000	0.0000	0.0000
O₂		0.1476	0.1476	0.1041	0.1041	0.0636	0.0636	0.0000	0.0000	0.0000	0.0000	0.0000	0.0000	0.0000	0.0000	0.0000
CO₂		0.0882	0.0882	0.1497	0.1497	0.2069	0.2069	0.1687	0.1350	0.1394	0.1368	0.1368	0.5092	0.5092	0.5092	0.5092
H₂S		0.0000	0.0000	0.0000	0.0000	0.0000	0.0000	0.0000	0.0000	0.0000	0.0000	0.0000	0.0000	0.0000	0.0000	0.0000
CH₄		0.0000	0.0000	0.0000	0.0000	0.0000	0.0000	0.0213	0.0173	0.0173	0.0173	0.0173	0.0642	0.0642	0.0642	0.0642
H₂O		0.0669	0.0669	0.1136	0.1136	0.1569	0.1569	0.0444	0.2271	0.2227	0.2253	0.2253	0.1340	0.1340	0.1340	0.1340
CO		0.0000	0.0000	0.0000	0.0000	0.0000	0.0000	0.0227	0.0201	0.0157	0.0184	0.0184	0.0684	0.0684	0.0684	0.0684
Mass Flows	kg/hr	26.919	26.919	30.019	30.019	33.525	33.525	41.944	35.104	23.330	58.434	58.434	36.660	10.164	7.275	19.222
Mass Fractions																
H₂		0.0000	0.0000	0.0000	0.0000	0.0000	0.0000	0.1400	0.1002	0.1009	0.1005	0.1005	0.0160	0.0160	0.0160	0.0160
N₂		0.6657	0.6657	0.5970	0.5970	0.5345	0.5345	0.0000	0.0000	0.0000	0.0000	0.0000	0.0000	0.0000	0.0000	0.0000
O₂		0.1610	0.1610	0.1122	0.1122	0.0678	0.0678	0.0000	0.0000	0.0000	0.0000	0.0000	0.0000	0.0000	0.0000	0.0000
CO₂		0.1323	0.1323	0.2220	0.2220	0.3034	0.3034	0.6940	0.4918	0.5078	0.4982	0.4982	0.7940	0.7940	0.7940	0.7940
H₂S		0.0000	0.0000	0.0000	0.0000	0.0000	0.0000	0.0000	0.0000	0.0000	0.0000	0.0000	0.0000	0.0000	0.0000	0.0000
CH₄		0.0000	0.0000	0.0000	0.0000	0.0000	0.0000	0.0319	0.0229	0.0229	0.0229	0.0229	0.0365	0.0365	0.0365	0.0365
H₂O		0.0411	0.0411	0.0689	0.0689	0.0942	0.0942	0.0748	0.3385	0.3319	0.3359	0.3359	0.0856	0.0856	0.0856	0.0856
CO		0.0000	0.0000	0.0000	0.0000	0.0000	0.0000	0.0593	0.0467	0.0364	0.0426	0.0426	0.0679	0.0679	0.0679	0.0679
Volume Flow	m³/hr	60.351	33.894	68.087	37.422	75.340	41.065	24.146	19.127	11.472	28.081	30.605	7.199	1.996	1.428	3.775

Table 9. MVP STARS process heat exchanger specifications.

Parameter	Units	3501	4501	3502	3503	3504	3505	4502	4503	4504	4505	4506
Inlet hot stream temperature	°C	785	785	549.9	571.9	522.4	313.6	550.0	561.3	554.5	308.3	96.5
Inlet hot stream pressure	bar	4.85	4.85	1.041	1.031	1.021	4.650	1.041	1.031	1.021	4.650	4.650
Inlet hot stream vapor fraction		1	1	1	1	1	1	1	1	1	1	0.959
Outlet hot stream temperature	°C	225.0	225.0	189.0	184.5	175.9	90.0	189.2	185.6	178.2	100.0	87.8
Outlet hot stream pressure	bar	4.75	4.75	1.041	1.031	1.021	4.650	1.041	1.031	1.021	4.650	4.650
Outlet hot stream vapor fraction		1	1	1	1	1	0.916	1	1	1	0.989	0.900
Inlet cold stream temperature	°C	141.2	141.2	139.0	134.5	125.9	24.0	139.2	135.6	128.2	94.2	24.0
Inlet cold stream pressure	bar	5	5	5	5	5	5	5	5	5	5	5
Inlet cold stream vapor fraction		0.989	0.989	0.838	0.655	0.478	0.252	0.852	0.691	0.513	0.299	0.252
Outlet cold stream temperature	°C	773.4	773.4	141.2	139.0	134.5	125.9	141.2	139.2	135.6	128.2	94.2
Outlet cold stream pressure	bar	4.95	4.95	5	5	5	5	5	5	5	5	5
Outlet cold stream vapor fraction		1	1	0.989	0.838	0.655	0.478	0.989	0.852	0.691	0.513	0.299
Heat duty	W	10336	15553	2202	2727	2733	5810	3007	3591	4107	5906	3660
UA	J/sec-K	351.07	527.34	12.90	15.37	16.57	117.33	17.61	20.59	23.67	232.05	198.82

2.3.2 WBS 2.0 STARS Improvements for Hydrogen Production and the Co-Production of Methanol and Hydrogen

2.3.2.1 SMR Reactor Refinement and On-Sun Testing

Design Improvements

The STARS reactor design was refined during 2017 to address issues identified for the TRL 6 design during the previous SunShot project. Specifically, the TRL 6 design featured a group of spiral reaction channels machined into the sun-facing plate and a group of counter-spiral heat recuperation channels machined into the opposite plate. The two plates were diffusion bonded to a common middle plate to complete the reactor vessel. The quality of the diffusion bonds was found to be sensitive to (1) the flatness and surface finish of the middle plate and (2) the limited areas where the counter spiraling channel walls overlap. The latter is related to bond quality because the load force during diffusion bonding can only clamp the plate together effectively over those overlapping spots. One example of the bond quality issue is shown by the ultrasonic scan image of an internal plane of the TRL 6 reactor (Figure 4). The missing, weakened or damaged internal bonds can lead to stress buildup on the reactor rim and premature failure and leakage.
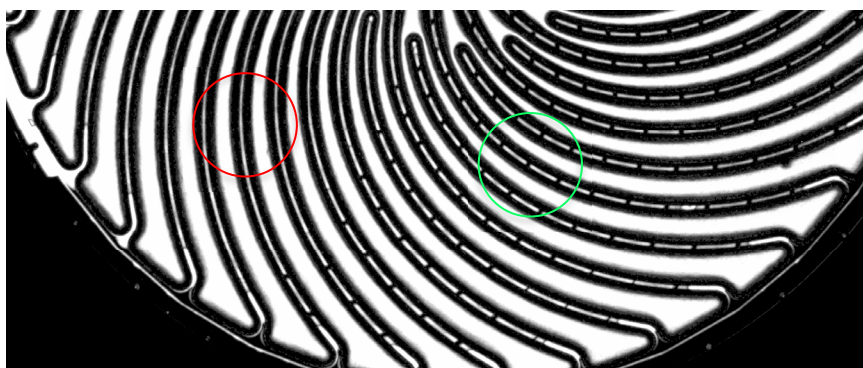
Figure 4. TRL 6 reactor ultrasonic microscopy scan image (C-scan top view using time gates, 20 MHz pulse echo with 5 MHz high pass filter). Green circle: normal diffusion bonds through the entire stack of reactor plates, indicated by the dark dots along channel spiral arcs. Red circle: absence of solid-solid bonds, indicated by the continuous spiral arcs.

The reactor design was modified to increase the effective bonding area internal to the reactor. This was achieved by changing the previously smooth spiral channel walls to have periodic circular pin reinforcements. The pin positions were aligned across the reactor plates so that during diffusion bonding the clamping load is transferred effectively through the entire stack. This enhancement was carefully balanced with the reduction of total volume for catalyst. In the final design, the through-thickness bonding area was increased to 2.4 times of that of the previous TRL 6 reactor, trading off 25% less catalyst volume and 16% more wall metal mass compared to the TRL 6 reactor. The rim and internal bonding areas of the two reactor designs are illustrated in Figure 5.
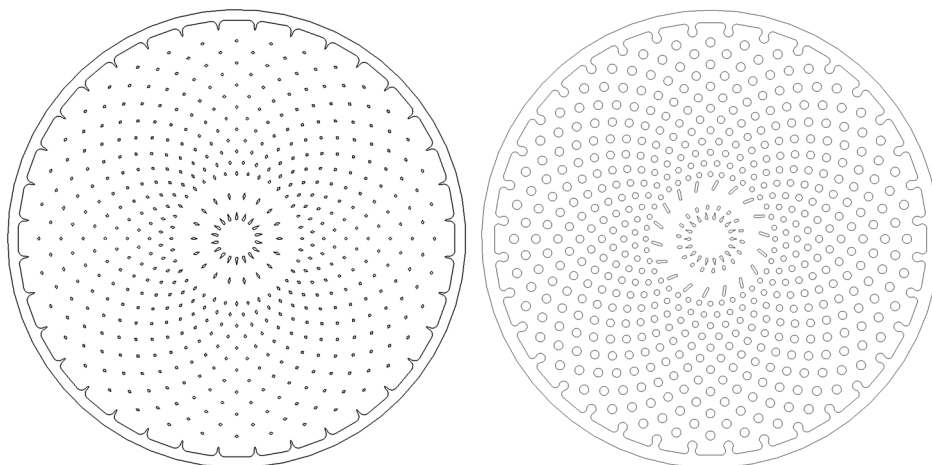
Figure 5. Projected through-bonding areas inside the TRL 6 (left) and TRL 7 (right) reactors.

An additional improvement was made to increase the design pressure of the SMR reactor from 10 bar to 20 bar to reduce compression work for downstream hydrogen purification and potential methanol synthesis. This was achieved by increasing the reactor plate thickness in addition to the enlarged internal bonding island areas. In the final design, the reactor mass was roughly doubled compared to the TRL 6 reactor. The structure of the TRL 7 reactor is shown in Figure 6.
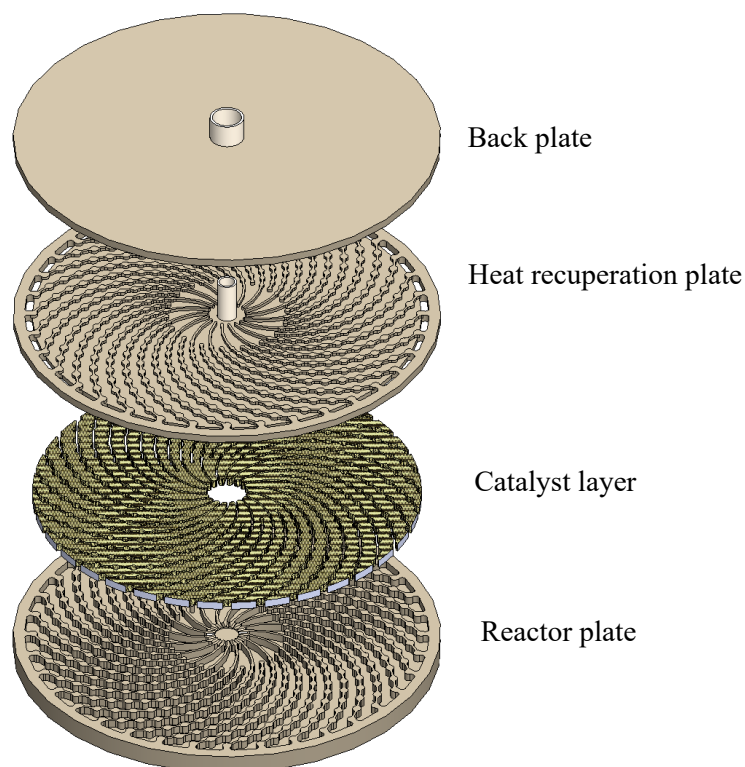
Figure 6. Exploded view of the TRL 7 reactor internal structure (the bottom face of the reactor plate, hidden, receives solar flux).

The structural mechanics of the new reactor design was evaluated by finite element simulations using custom built COMSOL Multiphysics models. The objectives of the modeling work were to achieve the design pressure target and to optimize reactor internal structure to reduce total mass and increase bond area. Taking advantage of the periodic symmetry of the counter spiral channel structures, only 1/18 slice of the reactor was modeled using periodic boundary conditions. Additional boundary conditions included constant heat flux on the reactor plate front surface equivalent to a PowerDish III concentrated solar (900W/m^2 over 14.85 m^2 total mirror area with 0.93 mirror reflectivity and 0.89 receiver intercept, or 11.0 kW-thermal total), 850°C on all internal surfaces of the reactor plate, 750°C on exterior face of the back plate, and 20 bar internal pressure. This model configuration without coupling the reactive flows was justified because the heat transfer boundary conditions were selected based on extensive flow simulations done on the TRL 6 reactors.

Coupled solid phase heat transfer and solid mechanics were solved over the 1/18 reactor slice domain to obtain von Mises stress values in the reactor body. Temperature-dependent allowable stress was looked up from ASME BPVC.II.D.C-2015, Table 1B, line 21 (alloy UNS N06230, solution annealed) for a range topped at 982°C. The curve was represented in COMSOL by piecewise linear interpolation. Temperature field was first solved independently based on 11 kW solar flux and a nominal 850°C reaction zone temperature. Next, displacement and local stress are then solved. Finally, the ratio of work stress to ASME allowable values was calculated at all discretized locations including several critical work planes corresponding to diffusion bonds or anticipated stress concentrations (Figure 7). This load ratio was then evaluated (Figure 8) with a global threshold of 0.95 to judge the reactor structure's ability to withstand the load. Based the finite element analysis the TRL 7 reactor was approved for testing to a 20 bar design pressure rating.
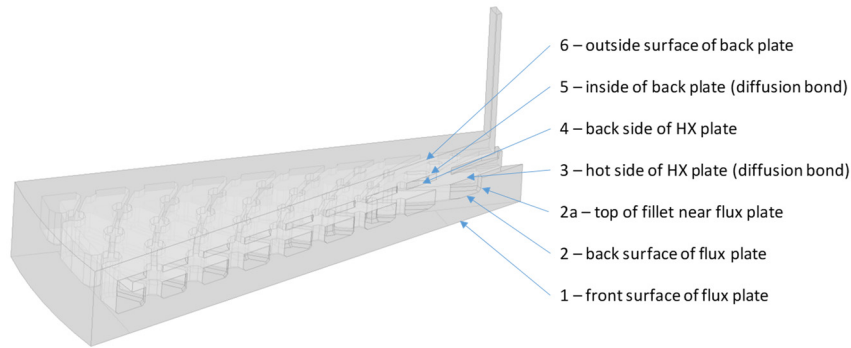

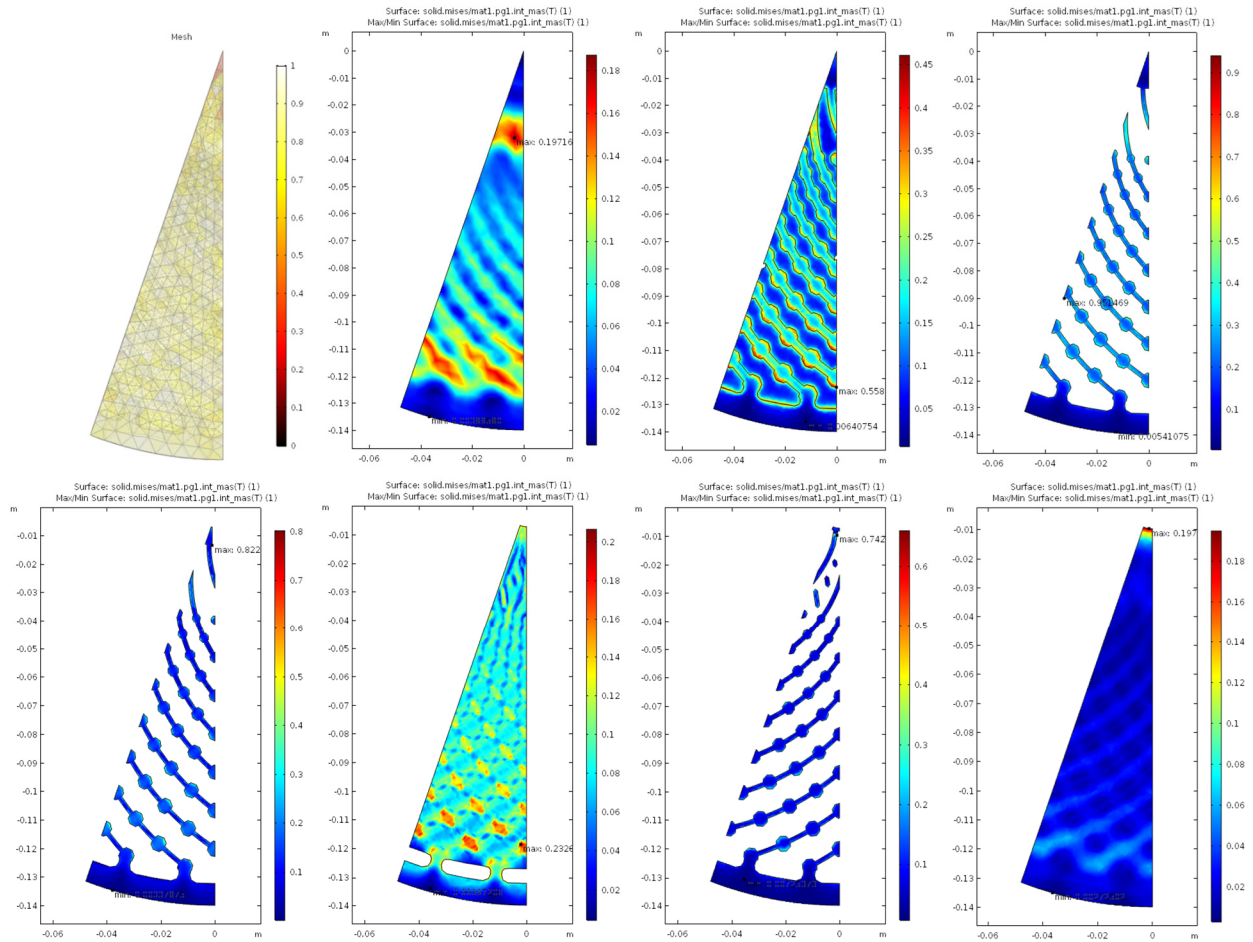**Figure 7.** Indices of work planes in the TRL 7 reactor model for solid mechanics simulations.

Figure 8. Simulation results plotted to show variations of load ratio (work stress divided by ASME allowable) in different work planes in the TRL 7 reactor body.

Fabrication

An improved fabrication process for the TRL 7 STARS reactor unit was developed during this project, building upon experiences and learnings from the previous SunShot project. The quality of the intermediate reactor parts was improved by adding a dual-dish grinding step to ensure the flatness of the reactor plates prior to diffusion bonding. The improved reactor design also eliminated a thin middle plate that had been found prone to deformation. An additional nondestructive evaluation was added after diffusion bonding to check for bonding defects by ultrasonic scanning microscopy. Finally, a formal intermediate quality assurance and final product acceptance process was adopted to document the reactor unit fabrication. The manufacturing flow diagram of the TRL 7 reactor unit is shown in Figure 9. The project team transferred the knowledge and experiences on using this process to STC. It was anticipated that STC would apply the learning to develop its own best-practice method for the manufacturing of STARS units for near term commercial applications. The fabrication process is explained in detail below.

16

Figure 9. TRL 7 STARS reactor unit fabrication steps (color coding: **grey**, raw materials; **blue**, subtractive manufacturing; **brown**, additive and assembly steps; **gold**, diagnosis and inspection; **green**, qualification).

The reactor and heat exchanger assembly were fabricated by April, 2018, according the finalized design. Photos of the reactor plates during various stages of the fabrication are presented in Figure 10. The reactor itself was fabricated from Haynes 230 alloy plates procured from Haynes International, Inc., to the specifications of AMS5878D. The plates were cut into shape by water-jetting and ground to a surface finish better than 24 micro inch and restrained parallel of 0.001 inch by a dual-dish grinding method.

Channels were machined into the reactor plates by CNC milling. After the machining step, the deforming of the plates and variations in channel depths were measured by profilometry and found within tolerances. Prior to diffusion bonding of the reactor plates, the plates were plated with a thin layer of nickel metal and the shaped rhodium catalyst inserts were placed into the reaction channels.

Catalyst foam substrate was fabricated from stock FeCrAlY foam boards (Selee Corporation, 50 ppi, 3% dense). The foam materials were cut into reactor channel shapes by wire electrical discharge

machining. A rhodium catalyst was coated onto the foam substrate according to the same procedure established during the previous SunShot project. A total of 23 g catalyst was loaded.
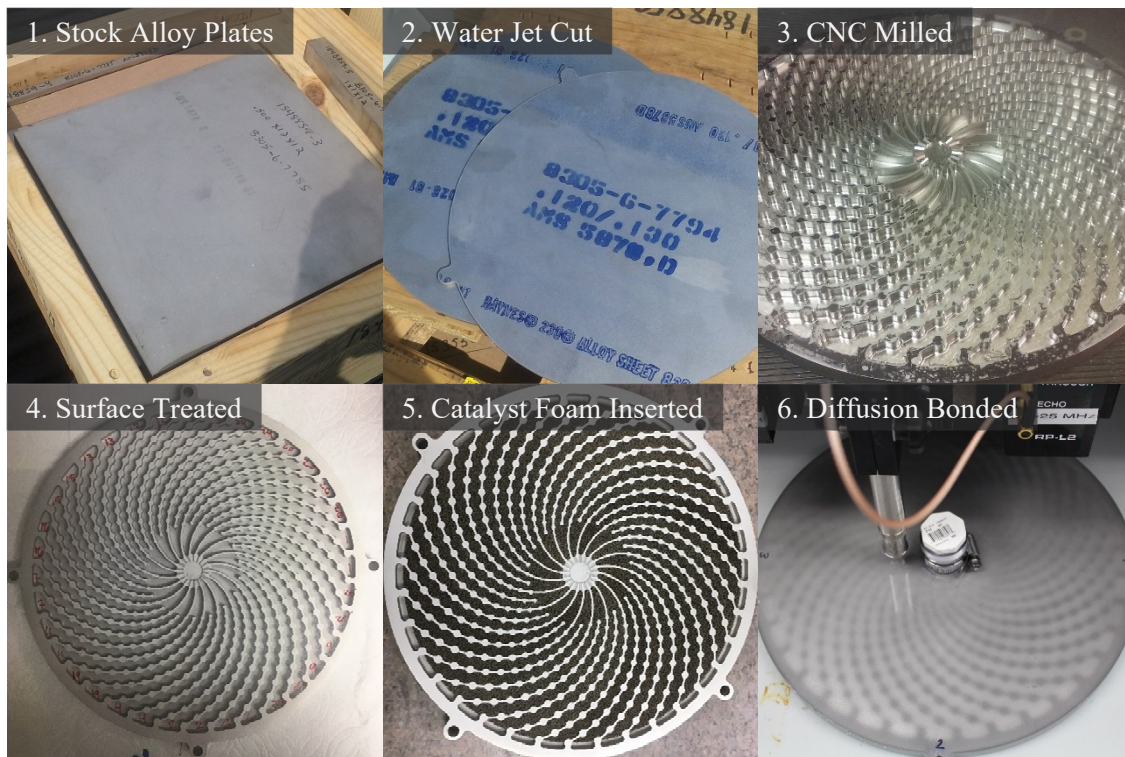

Figure 10. Photo images of the TRL 7 SMR reactor plates during various stages of fabrication.

After diffusion bonding, the reactor was checked for defects by helium inboard leak test and by an ultrasonic scanning microscope. Helium leak tested was performed per ASTM E498 method A, i.e., to spray helium tracer gas around the evacuated part. The bonded reactor was found to be leak tight to less than 1.0×10^{-9} std-cc/sec. The nondestructive scanning test revealed that the bonding quality was good between all three reactor plates. As shown in Figure 11, the ultrasonic imaging confirmed that continuous sound transmission paths existed in areas of intended bonding, indicating solid-solid bonding. The dark regions in the scan images, corresponding to solid material through the entire thickness of the reactor, can be compared to the projected through-thickness bond areas shown in Figure 5 with a very good match.
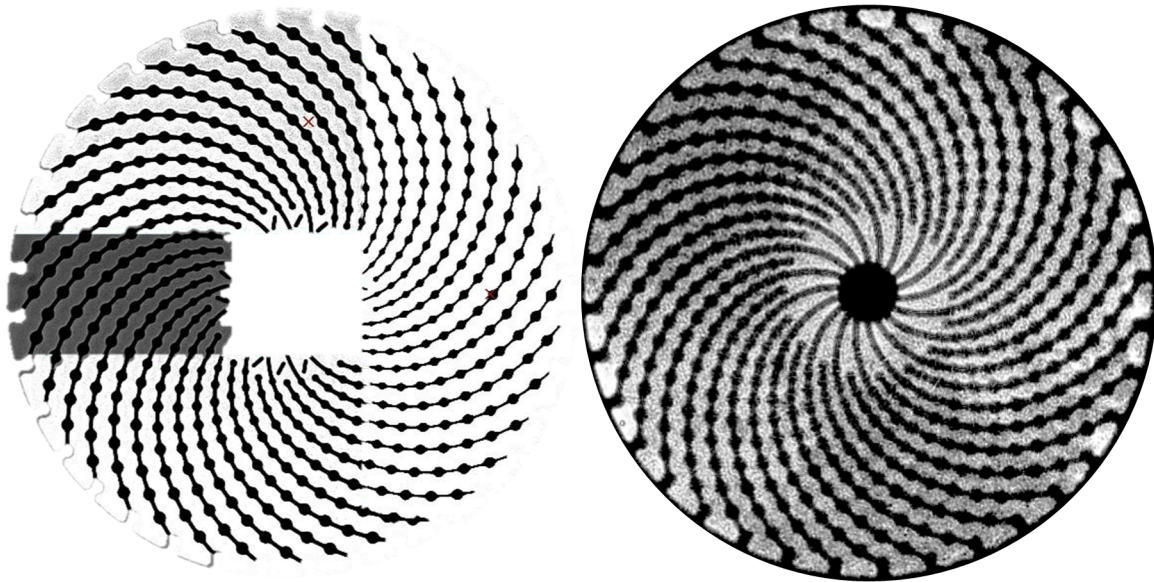
Figure 11. Ultrasonic scanning images of the TRL 7 SMR reactor (left, bond plane between the back plate and the middle plate; right, bond plane between the on-sun plate and the middle plate). Dark areas indicate defect-free solid bonds.

The diffusion bonded reactor was joined to a high temperature recuperator (HTR) by welding. The HTR and the necessary connection fittings were fabricated in Inconel 625 by laser powder bed fusion. The weld assembly of SMR-HTR reactor unit was tested for leakage using pressurized nitrogen gas. The reactor unit passed the leak test at 319 psig (1.1 times of the 20 bar design pressure) and was accepted as a completed build for further reactor testing.

The reactor unit was installed into the receiver nacelle of a PowerDish III parabolic dish solar concentrator. Instrumentation and thermal insulation were added to complete the TRL 7 Dish-STARS on-sun unit as shown in Figure 12. The control system for the TRL 7 Dish-STARS were rebuilt from the TRL 6 design with improvements to process instrumentation related to safety. In the receiver-reactor assembly, separate hydrogen and methane gas sensors were installed to provide input signals to process alarms and safety shutoff. Piping and instrument layout inside the on-sun unit were redesigned to better protect the process controller from process heat. As part of the TRL 7 reactor fabrication work, the balance of plant of the test site in Brawley, CA, was also serviced and upgraded to ensure reliable operation.

Figure 12. Photo images of the TRL 7 Dish-STARS reactor assembly (**a**, the reactor-heat exchanger assembly installed in the dish receiver nacelle; **b**, the reactor assembly with thermal insulations; **c**, the solar receiver-reactor unit and its internal layout).

On-Sun Testing

The new TRL 7 reactor's performance was tested on-sun using the Dish-STARS facility in Brawley, CA, during summers in 2018 and 2019. The Brawley Dish-STARS test pad, located at (32.9798N, 115.4863W), was established previously under the SunShot project and was restarted with equipment calibration and required maintenance and upgrades in early 2018. A photo of the TRL 8 reactor tested on-sun with the Brawley dish concentrator is shown in Figure 13. The parabolic dish (Infinia PowerDish III) had a total collector area of 14.85 m^2 and was able to deliver approximately 11 kW thermal energy to the reactor at peak sun.

On-sun calorimetry was performed to benchmark the parabolic dish solar concentrator. The Brawley dish intercept was determined to be 82%, indicating a small degradation of the optical accuracy of the mirror panels compared to the 87%-89% intercept measured on the SunShot project dish concentrator. The reduction in intercept was attributed to the effects of aging adhesives under the Brawley mirror panels. With the panels' additional years in service and the optical accuracy was considered acceptable. Analysis of subsequent solar thermochemical reactor testing data had taken into account of the updated intercept parameter.

Initial reactor on-sun testing was performed to shake down the test unit and fine tune start-up and shutdown procedures. The TRL 7 reactor was found to be leak free over daily on-sun cycles. The operational characteristics of this reactor was similar to the previous TRL 6 reactor. The reactor was able to reach operational temperature with a ramp rate of 20°C/min. A slower startup ramp rate was used typically, however, to be conservative.

Remaining reactor on-sun tests focused on measurement of the reactor's energy efficiencies and operation experiences over extended duration and cycles. Selected days of on-sun operating profiles are shown in Figure 14, Figure 15, and Figure 16, with a variety of solar and atmospheric conditions including clear skies, cloud transients, and dusty air. The reactor remained leak-free at 10 bar pressure after each on-sun cycle.

Figure 13. A photo of the TRL 7 Dish-STARS reactor assembly during on-sun operation in Brawley, California in 2018.
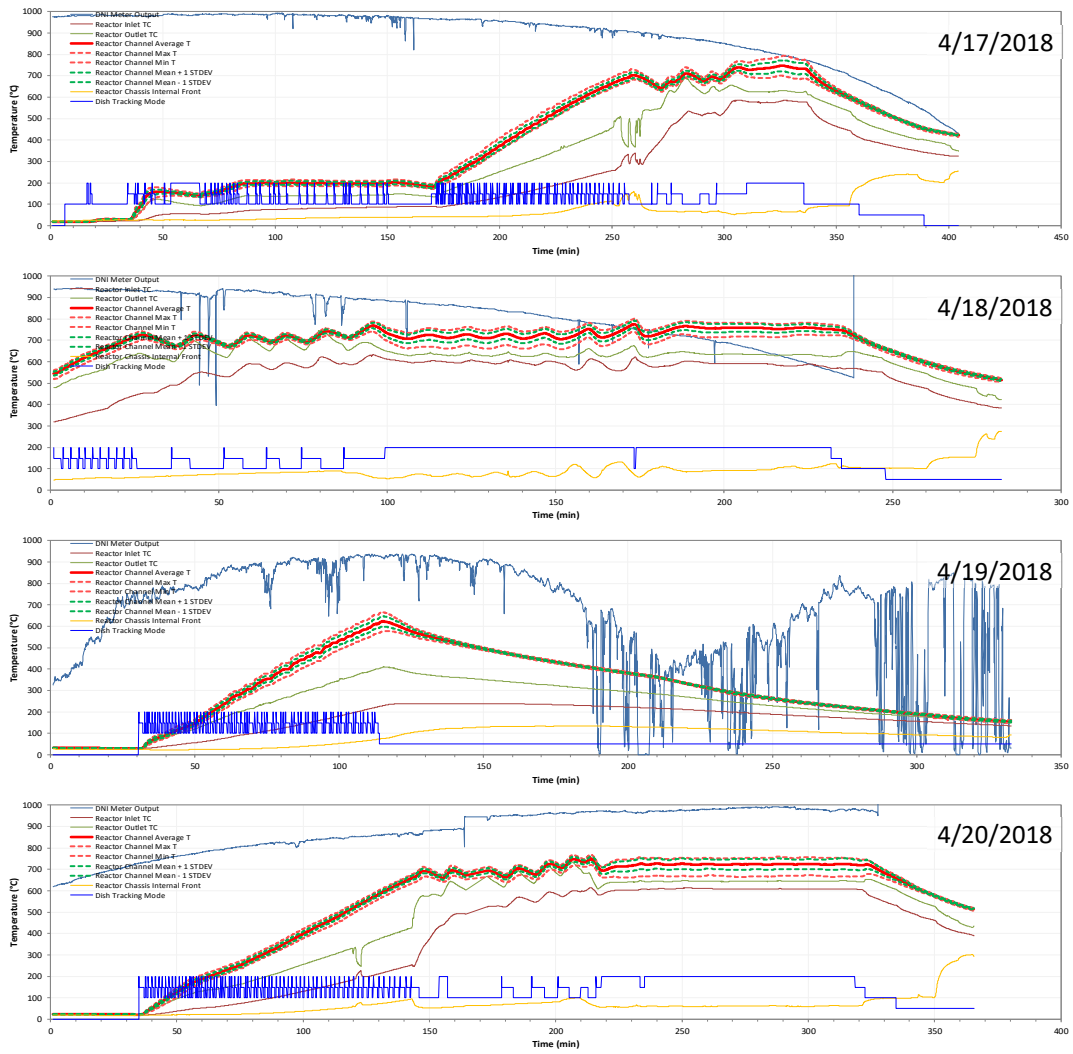
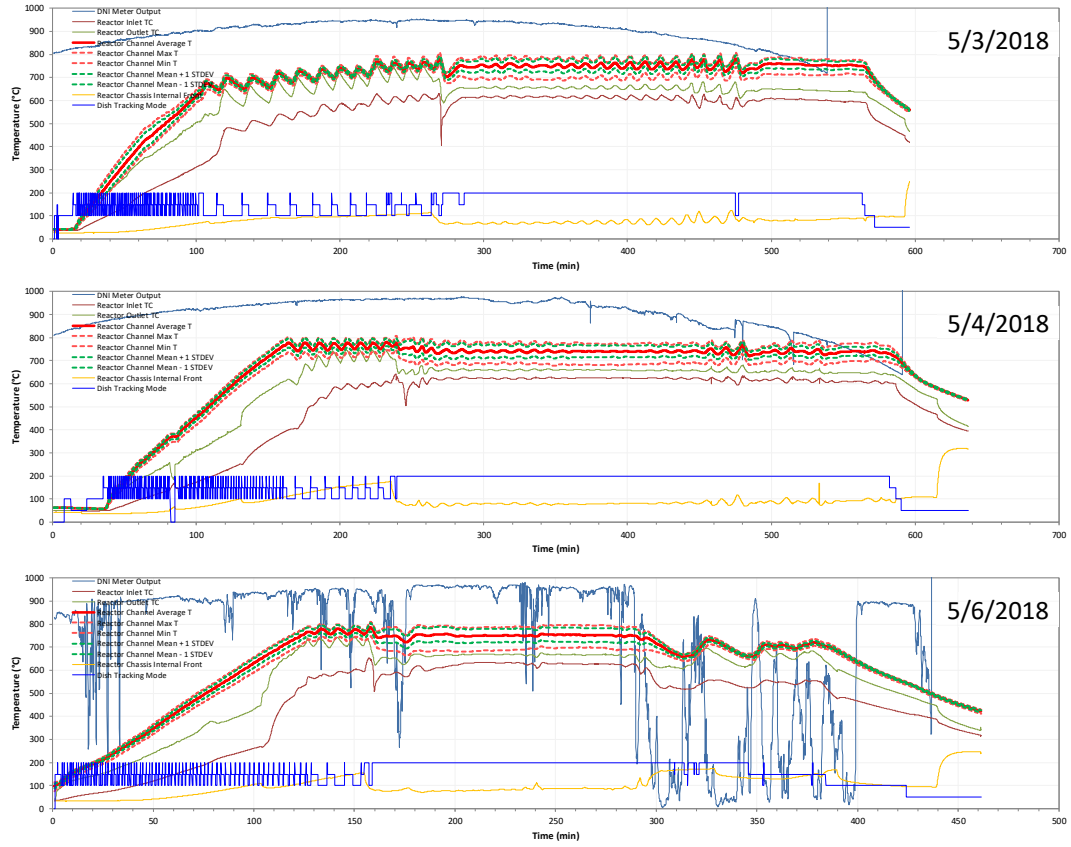**Figure 14.** TRL 7 reactor on-sun operating profiles on selected days (4/17/2018 to 4/20/2018).

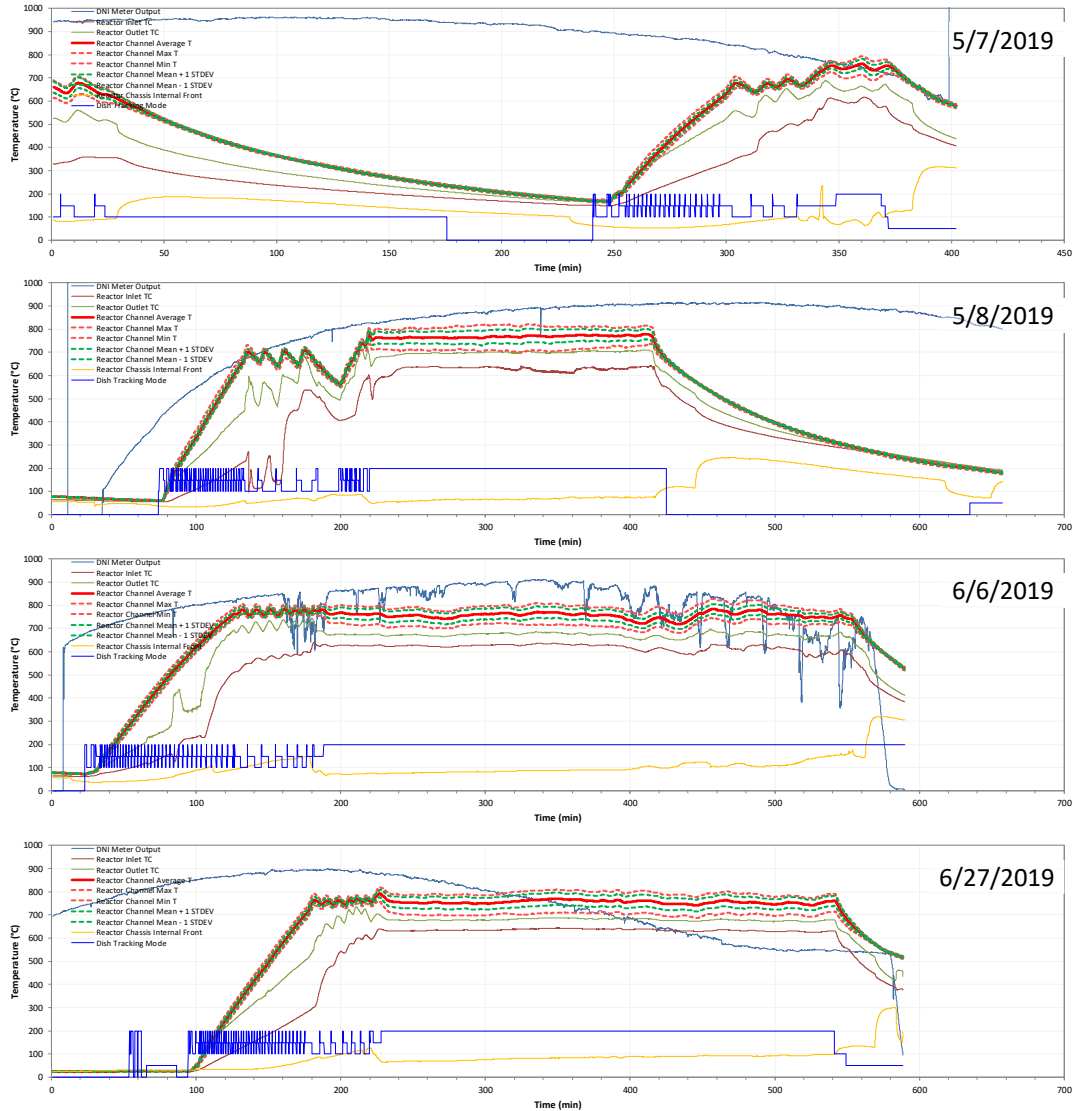**Figure 15.** TRL 7 reactor on-sun operating profiles on selected days (5/3/2018 to 5/6/2018).

Figure 16. TRL 7 reactor on-sun operating profiles on selected days (5/7/2019 to 6/27/2019).

The overall energy balance of the TRL 7 Dish-STARS receiver-reactor unit is shown in Figure 17, along with data on the similar TRL 6 unit from the previous SunShot project. The fixed heat losses of both systems were very similar, at approximately 1 kW-thermal, as indicated by the minimum solar receiver input power at an extrapolated zero reactor heat duty. This was expected because the TRL 7 reactor form factor (diameter and thickness) was very similar to the TRL 6 reactor and additionally the reactor mounting hardware and thermal insulation were the same.

Reactor thermal-to-chemical energy efficiency, which excludes energy losses due to dish optical error and receiver thermal loss, was well over 90% (Figure 18). This shows how superior the microchannel STARS reactor design was. This success can be attributed to two critical design features. First, the built-in heat recuperation channels in the reactor minimized exergy destruction and allowed the SMR reaction to finish at a thermodynamically advantageous higher temperature. Second, the counter-cross arrangement of the reaction and recuperation channels did a great job of spreading heat over large area of the reactor, compensating the optical imperfections of the dish concentrator and the tendency to create hot

25

spots. This minimized additional exergy destruction that might arise from uneven temperature and flow distribution among the reaction channels.

TRL 7 reactor achieved over 70% solar-to-chemical energy efficiency. From Figure 19, it can be observed that the TRL 7 reactor obtained slightly higher energy efficiency reactor at low to medium solar flux than the TRL 6 reactor. At high solar fluxes, both reactors exhibited similar energy efficiencies. Because the Brawley dish concentrator had a relatively low intercept (82%), a better dish concentrator would have allowed the TRL 7 reactor system to achieve a higher solar-to-chemical efficiency. Future improvement can be made by pairing the STARS reactor with a high-performance dish (>90% intercept) and potentially elevate the Dish-STARS solar-to-chemical efficiency to 73%-75% level.

The original test plan for the TRL 7 reactor called for a total of 300 hours of on-sun operation. The 2018 summer test campaign was completed successfully including the initial Brawley site restart, dish concentration re-calibration, and reactor on-sun tests. The 2019 late spring on-sun campaign was interrupted due to a dish concentrator equipment issue. A tracking error of the dish concentrator halted planned on-sun test runs. After additional onsite diagnosis, the error was later traced to a GPS rollover event which affects the ability of older GPS receivers to keep date and time correctly from April 6, 2019, and onwards. After the GPS receiver on the dish concentrator was replaced, the dish was recommissioned, and the reactor test stand was operational again. Subsequent on-sun tests planned for spring 2020 was called off when COVID-19 pandemic started, and travel restrictions were put in place by the U.S. Department of Energy. After discussion with the DOE Office of Solar Technology program manager, it was agreed that the project should not be extend beyond 12/31/2020. Significant number of on-sun hours were still accumulated. Total on-sun operation hours by the TRL 7 reactor was over 100 hours.
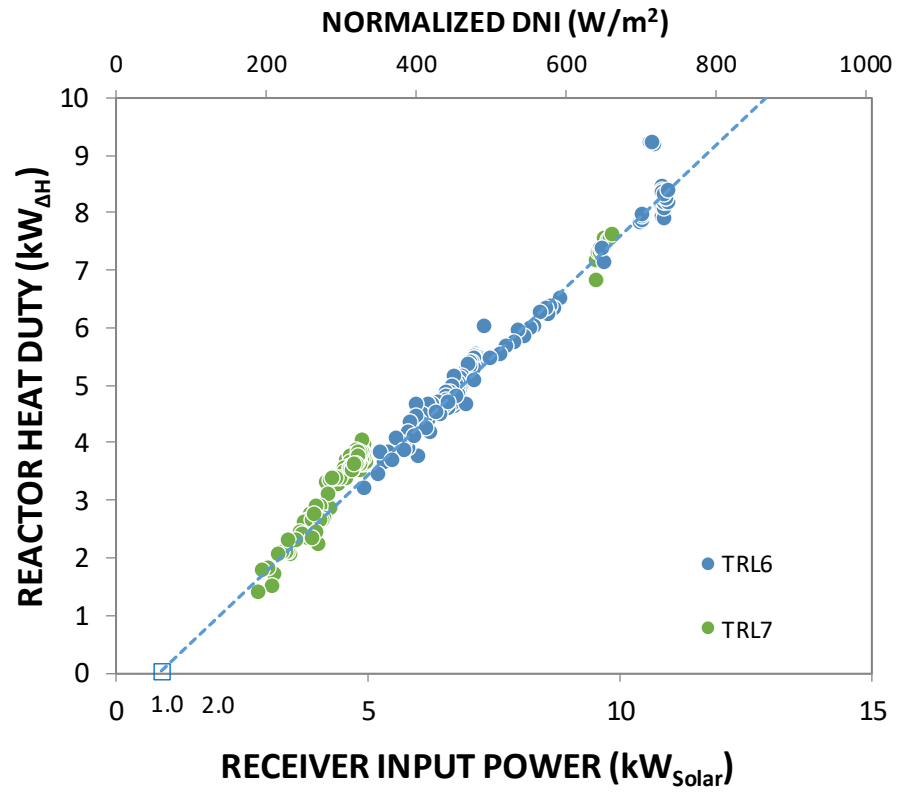
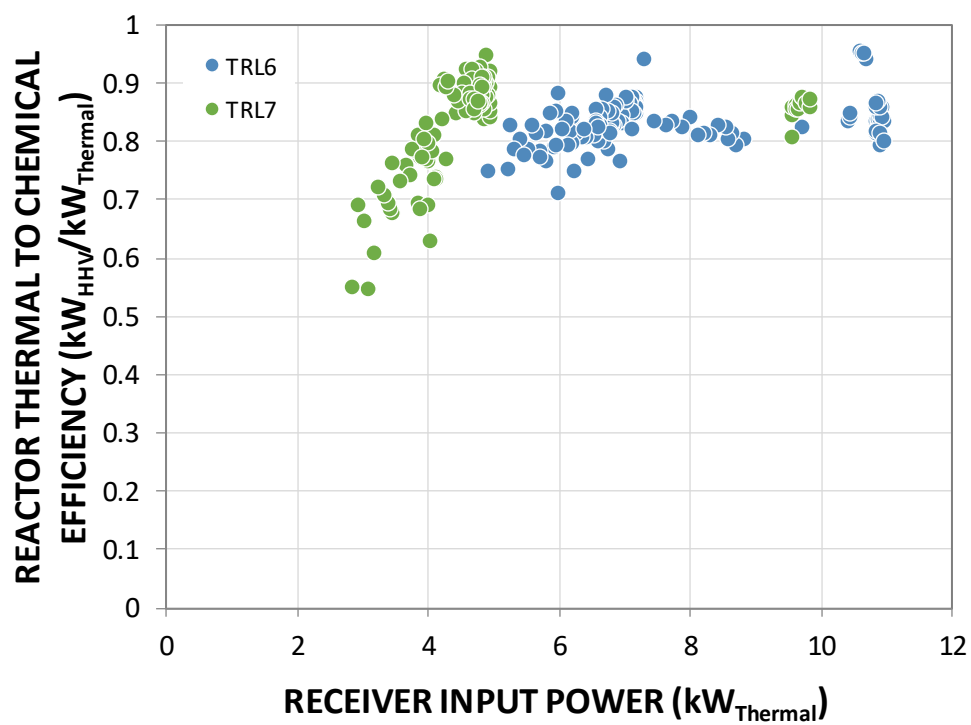**Figure 17.** Dish-STARS reactor on-sun heat duties vs. receiver input power.

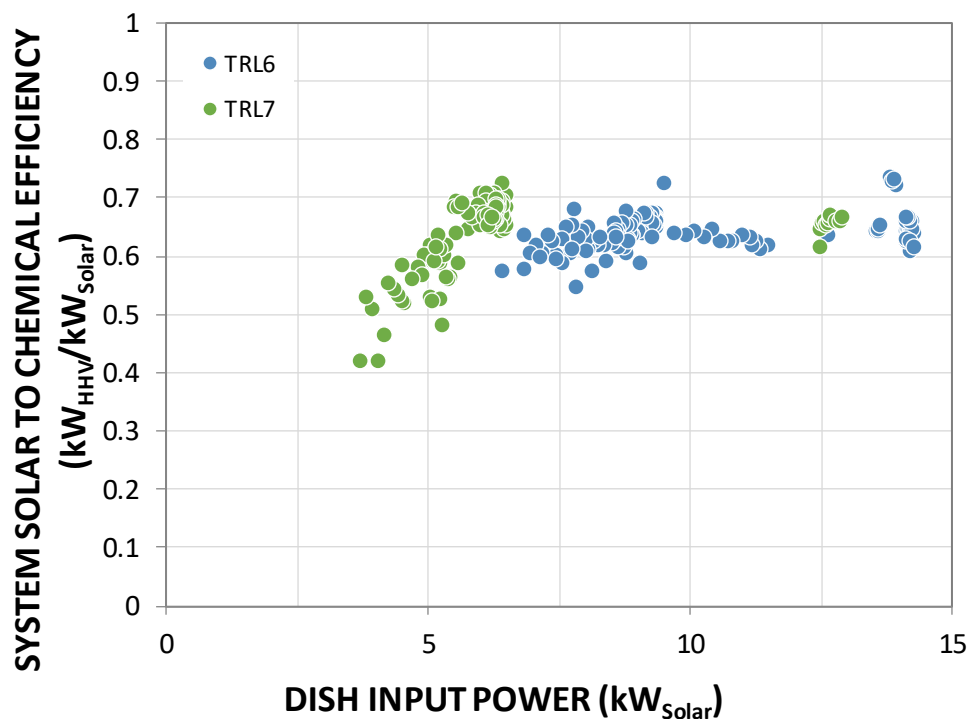**Figure 18.** Dish-STARS reactor thermal to chemical energy efficiency at various thermal input power.

Figure 19. Dish-STARS reactor system solar to chemical energy efficiency at various solar input power.

2.3.2.2 Water Gas Shift Catalyst Evaluation

Extensive flowsheet studies were performed from late 2017 to early 2018 to select the appropriate conditions for the water gas shift (WGS) reactors as part of the TRL 7 STARS overall design. The chosen reactor conditions were then used to aid the selection of WGS catalysts from commercial offerings. The selected WGS reactor design conditions are summarized in Table 10. Details of the study are included in this section.

Table 10. WGS reactor design data selected for the TRL 7 STARS process.

Stage	High Temperature WGS Reactor		Low Temperature WGS Reactor	
	Inlet	Outlet	Inlet	Outlet
T, °C	275	353	180	227
P, bar	11.8		11.8	
Mol Fractions	Inlet	Outlet	Inlet	Outlet
H_2	0.5105	0.5791	0.1210	0.1689
H_2O	0.2902	0.2215	0.4627	0.4147
CO	0.0947	0.0260	0.0544	0.0064
CO_2	0.0566	0.1253	0.2616	0.3096
CH_4	0.0481	0.0481	0.1004	0.1004

This above study was done according to the initial MVP design specifications (Section 2.3.1.2). Notably, this initial MVP design included a hydrogen membrane separator unit. The WGS evaluation refined the MVP design to place this hydrogen membrane separator downstream of a first-state high-temperature WGS reactor and upstream of a second-stage low-temperature WGS reactor. The reduced hydrogen concentration in the feed stream to the second-stage reactor helped to shift the equilibrium in the second WGS stage to higher conversion.

The design envisioned a separate WGS unit for each STARS SMR reactor with the reactors and heat exchangers housed inside the sun-tracking nacelle of the dish concentrator. The second stage was set to a 180°C inlet temperature to maximize the possible conversion. However, further optimization of this temperature was recommended if the catalyst quantity needed exceeds the limit on weight and size by the dish concentrator on-sun unit.

The minimum steam-to-carbon ratios (S/C) to avoid carbon formation were evaluated as a part of the WGS flowsheet modeling. This was done by allowing solid carbon to be a product in adiabatic Gibbs reactor calculations. S/C above 1.0 was found sufficient to avoid carbon formation in the reformer running at 800°C and the first WGS reactor. S/C a S:C ratio at least 2.3 was found necessary to avoid carbon at the exit of the membrane separator and the second WGS reactor. At the lower temperature locations there was significant methanation reaction and heating of the mixture when it was equilibrated. However, the Gibbs equilibrium was still a reasonable test for carbon forming potential. Based on the above results, S/C of 2.5 was used in the flowsheet to obtain the WGS reactor design information. Other key assumptions included 90% approach to equilibrium of the adiabatic WGS stages and 90% hydrogen recovery after the first shift reactor.

2.3.2.3 Methanol Synthesis Catalyst Evaluation

The Dish-STARS process can be used to make fuels and chemicals beyond syngas and hydrogen. Integration with methanol synthesis had been identified as one of such opportunities for near-term Dish-STARS applications. During the early phase of this project, an experimental study was conducted using single channel reactor testing to evaluate commercial a Cu/ZnO catalyst for methanol synthesis. The test results including catalyst stability and reaction kinetics are summarized in this section. No further development of the methanol synthesis integration was done under the current project because the team had focused the near-term commercialization effort on a hydrogen production application at FCV filling stations.

Methanol synthesis catalyst and single channel reactor

The methanol synthesis catalyst evaluated was a commercial Cu/ZnO formulation with Al_2O_3 support. Copper was greater than 50 mol% of the metal phase. The active phase consisted of approximately spherical Cu nanoparticles of a size around 10 nm mingled with ZnO nanoparticles in a porous aggregate. The Cu surface area was approximately 40 m^2/g. The catalyst can be deactivated by sintering which is acerated by high temperature.

The single channel reactor testing was done with 1 g batches of the catalyst diluted in 10 g of SiC loaded inside a stainless steel tube of 3/8" outside diameter. The reactor was equipped with multiple temperature sensors located in the catalyst bed, at the reactor wall, and at reactor inlet. A schematic of the

reactor test stand is shown in Figure 20. A feed gas with blended CO, CO_2, and H_2 compositions was mixed with steam and fed to the reactor tube. The reactor temperature was controlled by the furnace temperature controller. The bed temperature can vary by 2-3 ºC due to changes in the contact time and the exothermic reaction rate. The reaction product was chilled and separated into gas and liquid in a cold trap before the gas phase was vented via a back pressure control valve.
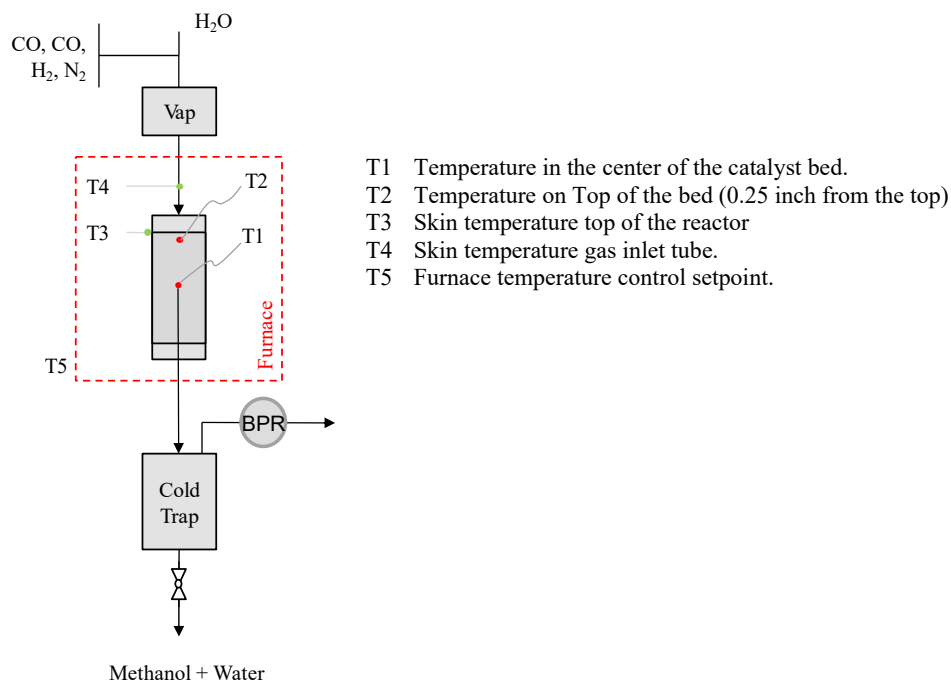

T1 Temperature in the center of the catalyst bed.
T2 Temperature on Top of the bed (0.25 inch from the top)
T3 Skin temperature top of the reactor
T4 Skin temperature gas inlet tube.
T5 Furnace temperature control setpoint.

Figure 20. Schematic of single channel reactor test stand for methanol synthesis catalyst evaluation.

Catalyst stability over CO₂ and water

Effects of CO_2 on catalyst stability were studied by single channel reactor tests at 500 psig and a constant GHSV of 6800 hr^{-1}. The H_2 and CO mole fractions in the feed were kept constant at 0.54 and 0.27, respectively. Feed CO_2 and N_2 compositions were varied. The effects of CO_2 feed concentration on the CO conversion and catalyst deactivation are shown in Figure 21 and Figure 22. Catalyst activity was checked after a sequence of increasing CO_2 feed concentration. Decrease by 73% and 25% in CO conversion was found at 230°C and 250°C, respectively, under low CO_2 concentrations. At higher CO_2 concentrations, simulating a methanol synthesis feed with recycled CO_2, acute deactivation was found. It was concluded that the catalyst was not stable with CO_2 rich feeds.
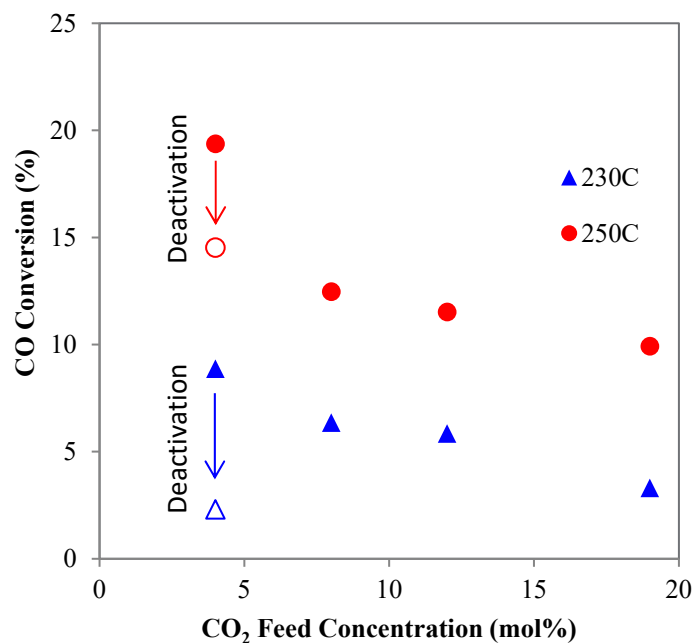
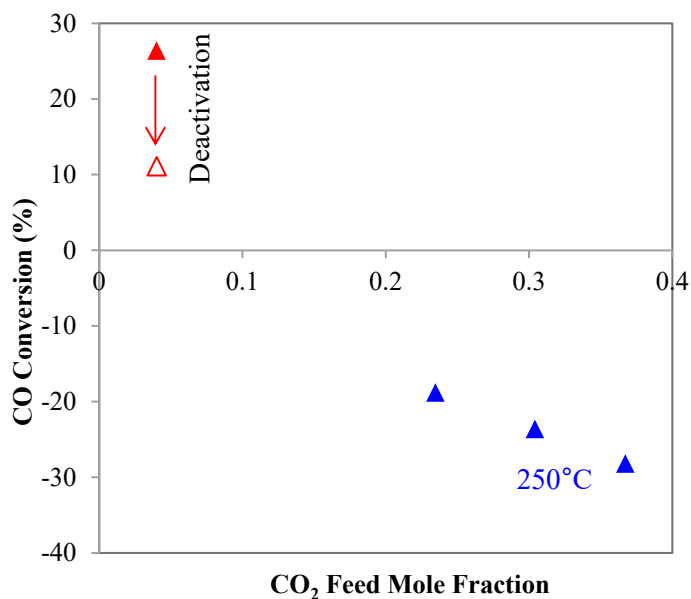**Figure 21.** Effects of low CO_2 feed composition on CO conversion (500 psig, GHSV 6800 hr^{-1}).

Figure 22. Effects of high CO_2 feed composition on CO conversion (500 psig, GHSV 6800 hr^{-1}).

Effects of water on catalyst stability were studied by additional single channel reactor tests at 500 psig, 250°C, and a constant GHSV of 6800 hr^{-1}. The H_2, CO, and CO_2 mole fractions in the feed were kept constant at 0.54, 0.05, and 0.21, respectively. Feed H_2O and N_2 compositions were varied. The effects of H_2O mole fraction on CO conversion are shown in Figure 23. WGS reaction was promoted with water in the feed; however, acute deactivation was found after returning to the checkpoint.
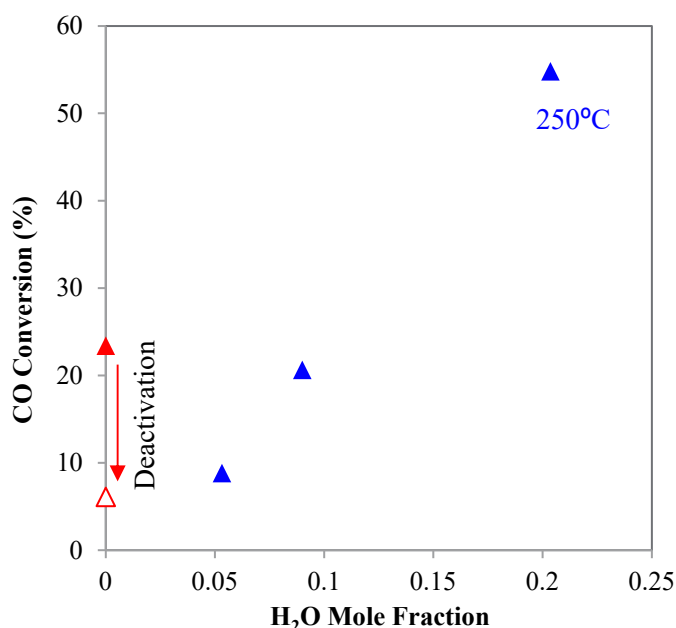
Figure 23. Effects of H_2O mole fractions on CO conversion (500 psig, GHSV 6800 hr^{-1}).

The above single channel catalyst data can be compared with published literature. Deactivation has been reported to be related to water formation and CO_2 itself facilitating sintering of Cu particles [1]. Water and CO_2 negatively affected catalyst stability according to Fichtl et. al. recent kinetic deactivation model on a commercial catalyst [2]. Silica or zirconia are more stable supports to choose for CO_2 hydrogenation [3]. Bell et al. [4] reported that CO_2 hydrogenation was faster than CO hydrogenation as an effect of zirconia addition and that zirconia and silica catalyst supports were more stable than alumina supports.

Conversion under methanol synthesis baseline conditions

The performance of the methanol synthesis catalyst was evaluated by parametric testing at a set of standard feed compositions assuming post-SMR equilibrium conditions (800ºC, 15 bar, S/C=2.5) and after water condensation: 72.4% H_2, 13.5 CO, 9.1% CO_2, 0% H_2O, and 5% N_2 by moles. The testing was designed to assess CO conversion as a function of reactor temperature and space velocity and to obtain a kinetic expression. As shown in Figure 24 the CO conversion approached equilibrium and CO2 conversion decreased at high temperatures. Methanol yield approached the equilibrium at high temperatures as shown in Figure 25. The catalyst did not show deactivation in a single run; however, checkpoint (empty symbol in Figure 25) showed 18% deactivation post the test sequence to 270ºC. Analysis of the liquid samples collected in the 270ºC runs showed that the liquid water content was: 4.2, 3.8, and 5.3 weight percent (balance methanol) for 3500, 7000, and 21000 h^{-1} space velocity, or 1.0, 0.5, and 0.2 s contact time, respectively. Methanol formation over the catalyst was hampered by WGS reaction at high temperatures and low contact times based on the above results.
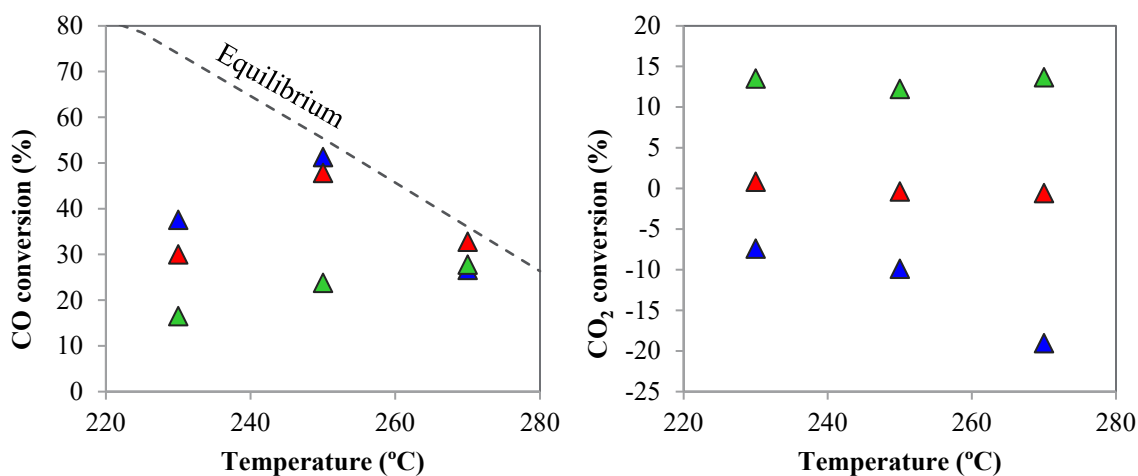
33

Figure 24. Effects of temperature and space velocity on methanol synthesis conversion at 500 psig (3500 h^{-1}, blue; 7000 h^{-1}, red; 21000 h^{-1}, green).

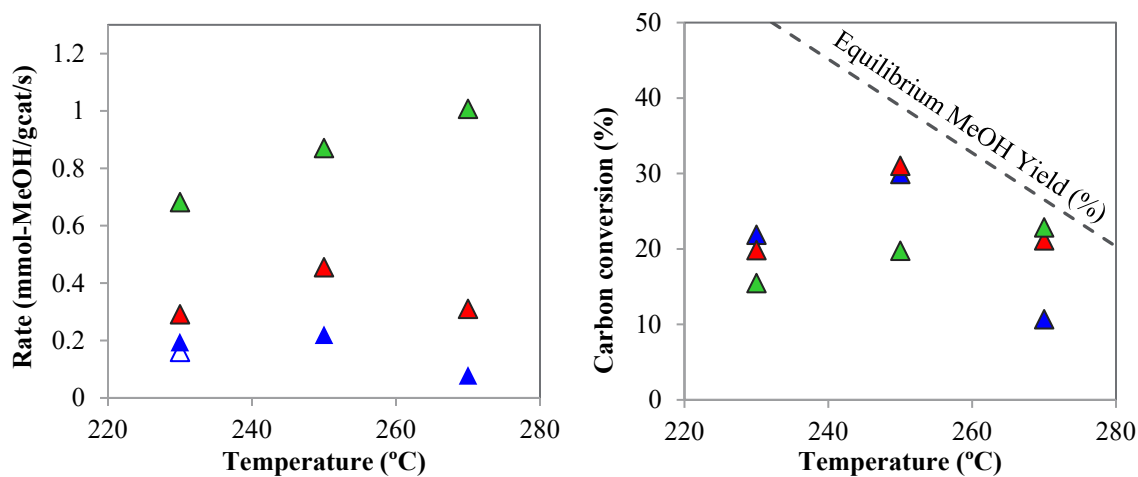**Figure 25.** Effects of temperature and space velocity on rate of methanol formation and total carbon (CO+CO$_2$) conversion at 500 psig (3500 h^{-1}, blue; 7000 h^{-1}, red; 21000 h^{-1}, green).

Catalyst stability over extended operation

The stability of this catalyst was tested during an extended hour operation with the methanol synthesis baseline feed composition (72.4% H_2, 13.5 CO, 9.1% CO_2, 0% H_2O, and 5% N_2 by moles) at 250°C and 500 psig. Overall carbon balance was 93%. The collected methanol liquid product contained 5% water. Far from the equilibrium and using a SMR model feed (9% CO_2), the catalyst demonstrated good stability during 48 hours on stream as shown in Figure 26.
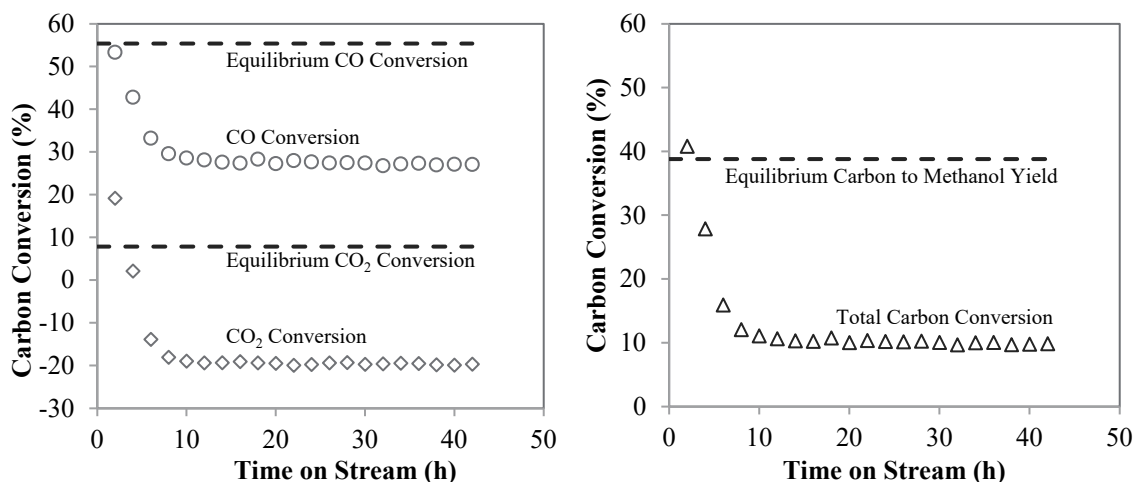
Figure 26. Carbon conversions during 48-hour methanol synthesis test at 250°C, 500 psig, and 7000 h^{-1} GHSV ($\tau = 0.25s$).

Kinetic rate expression measurements

Additional measurements were done to collect methanol synthesis kinetics data (Figure 27). By fitting the data at lower temperatures to Arrhenius plot, the reaction orders with respect to H_2 and CO were estimated to be 1.8 and 2, respectively. These were similar to generally reported reaction orders in literature for CO (0.2-1.0) and H_2 (1.0-2.0), respectively. CO_2 and H_2O were determined to be not kinetically relevant and were not included in rate expressions. The activation energy, E_a, was estimated to be = 73 kJ/mol. The reaction rate constant, k_o, was estimated to be 6.61 mmol/gcat/h.
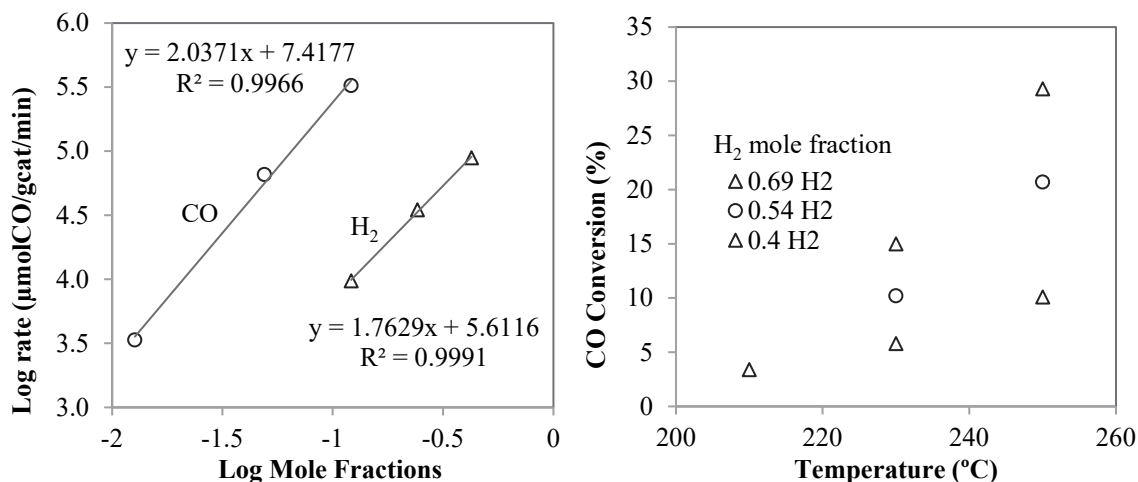

Figure 27. Methanol kinetics measurements at 500 psig and 6804 h^{-1} GHSV: left, 230°C; right, variable temperatures.

2.3.2.4   Catalytic Oxidation Steam Generator

An application of the STARS technology platform was identified by SoCalGas and STC for near-term demonstration of hydrogen production at FCV filling stations. Supporting the hydrogen production demonstration, a high efficiency vaporizer was designed under this project for steam generation using the

residual energy content of PSA tail gas in the STARS process. The goal of the design was to develop a catalytic oxidation steam generator (COSG) for the purpose of vaporizing water into medium- to high-pressure steam, using high-efficiency microchannel hardware and heat from the catalytic oxidation of the tail gas stream from a syngas-to-hydrogen separation unit. The objectives included: (1) achieving 26.5 kW/module heat duty delivering superheated steam at 14.1 bara and 225°C, (2) obtaining high heat transfer density and reducing device size through the use of a microchannel cross flow architecture, (3) controlling NO_x production to levels at 5 ppm (measured as NO_2) or lower using multiple stages of catalytic combustion, and (4) identifying designs suitable for metal additive manufacturing using the laser powder-bed fusion (LPBF) process, otherwise known as selective laser melting. The microchannel vaporizer was designed by PNNL with input from STC. The catalytic burner design was completed by a subcontractor of STC. The vaporizer and burner integration were designed to the same scale and compatible footprints, but the actual integration had been left for the follow-on commercial demonstration project. This section summarized the design details of the microchannel vaporizer.

The team evaluated relevant prior microchannel steam vaporizer designs by PNNL, particularly the panel vaporizer designs from 2000's, and adapted a basic design for the current project in terms of microchannel architecture, material of construction, combustion cell, and air side manifold. Heat transfer, pressure drop, and stress mechanics calculations were carried out to determine channel dimensions and wall thickness needed. Water channel orifice feature was designed based on steam channel pressure drop over the design flow range. Overall device footprint was estimated from the target scale and preliminary manifold and vessel design. CAD models of the vaporizer was created to move the design to fabrication.

After CAD models of the vaporizer were created, the design was finalized in sufficient manufacturing details to obtain fabricator budgetary quote. PNNL worked with STC to select potential LPBF vendor(s) to identify maximum printer build volume for the specific metal chosen. The vaporizer design was finetuned to ensure that the vaporizer section can be printed within the build volume and that the critical features cab be printed with fidelity. The optimization included adjustments in print orientation, internal channel dimensions, and header size and shape. The tooling features of the design were reviewed such as those aiding powder removal and registration of post-processing steps such wire EDM and welding. Prototypes were printed by a LPBF vendor to validate build quality.

Details of the above vaporizer and burner designs are not included in this report because a patent application is being pursued.

2.3.3 WBS 3.0 Balance of Plant Design

This task included the conceptual design of the hydrogen production and the co-production systems, to define subsystem and component requirements that were "outside the nacelle". This included discussions with vendors for balance of plant components, such as the PSA subsystem, that do require little or no technology development.

2.3.3.1 Conceptual Design of Hydrogen Production System

A joint project workshop was held in August 2018 with PNNL TCF and RAPID teams, STARS Technology Corp, and SoCalGas. An initial design was identified to target a proposal to California South

Coast Air Quality Management District (SCAQMD) for the first commercial demonstration of STARS hydrogen plant at fuel cell vehicle filling station. The commercial design specifications and Minimum Viable Product (MVP) process flowsheet from WBS 1.0 were updated based on specific targets for a near-term demonstration for SCAQMD at 120 kg-H_2/day scale. Aspen Plus and CHEMCAD process modeling was conducted for a hydrogen plant with multiple solar Dish-STARS^{TM} units, multiple induction heating electrical STARS units, a single water gas shift reactor, pressure swing adsorption unit for hydrogen separation, and tail gas combustion-based steam generation. The Front-End Loading Level 1 (FEL-1) flowsheet for the conceptual design was finalized by the end of 2018 with input from PNNL, SoCalGas, and STC. The scale of the FEL-1 design was adjusted to 165 kg-H_2/day based on STC near-term commercial development goal and was given the designation STARS-165. Table 11 lists the key specifications of this design. The process block diagram of the conceptual design is shown in Figure 28. The CHEMCAD flowsheet is shown in Figure 29. The FEL-1 conceptual design was picked up by SoCalGas and STC for further development into the detailed design of the target demonstration, which was outside of the current project.

Table 11. Key specifications of FEL-1 conceptual design (STARS-165).

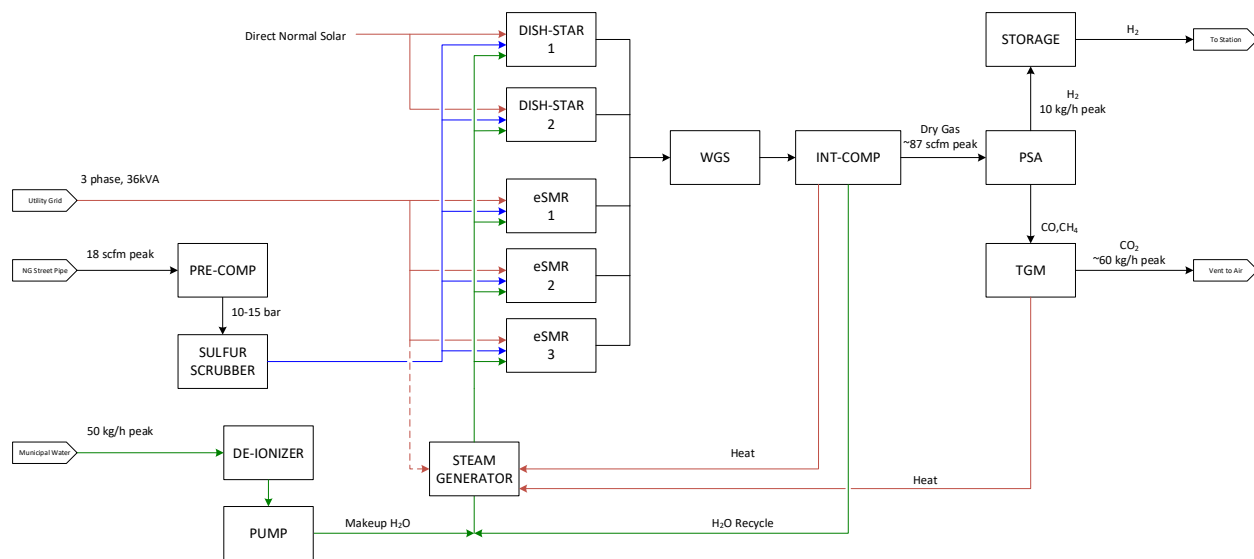| Parameters	Value
Hydrogen production rate, kg/day (peak hour)	165
Solar SMR methane conversion	90% at 800°C, 5-15 bar, 3:1 steam/carbon ratio
Electrical induction SMR methane conversion	90% at 800°C, 5-15 bar, 3:1 steam/carbon ratio
WGS conversion	90% at 225°C inlet
Number of solar SMR reactors	2
Parabolic solar concentrator	Infinia PowerDish III
Number of electric heating SMR reactors	3
Hydrogen separation	Pressure swing adsorption
PSA hydrogen recovery	90%
Steam generation	PSA tail gas combustion
Combustor temperature	550°C
Heat exchanger minimum approach, °C	15

Figure 28. Process block diagram of the FEL-1 conceptual design for hydrogen production.
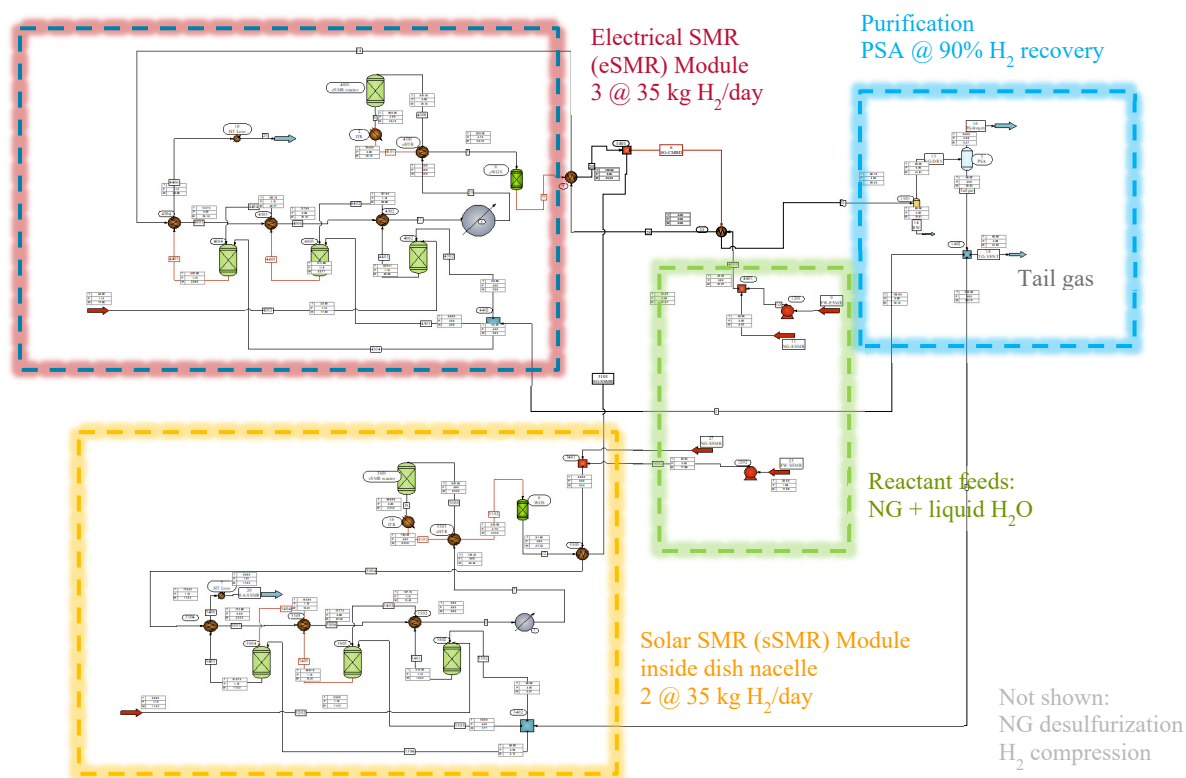

Figure 29. CHEMCAD flowsheet of the FEL-1 conceptual design for hydrogen production.

2.3.3.2　Technoeconomic Evaluation of Hydrogen Production System

TEA Analytical Approach and Key Assumptions

A technoeconomic analysis (TEA) was conducted by STC to produce cost projections of the hydrogen plant based on the above conceptual design at an industrial scale. The characteristics of the modeled hydrogen plant are summarized in Table 12. The analysis followed the economic methodology and assumptions defined by the DOE Hydrogen and Fuel Cell Technology Office. The solar/electric hybrid plant was assumed to operate continuously with a 30-year plant life. The SMR reactor life was assumed to be 7.5 years. The HTR heat exchanger life was assumed to be 15 years. Reactor and heat exchanger manufacturing costs were estimated based on 10,000 SMR units per year volume. Dish concentrator costs were based on Infinia estimates. Other distributed component costs were based on small-lot vendor quotes with discounts. Central component costs were based on vendor estimates. Solar input was based on DNI for Phoenix, AZ (2519 kWh/year). Utilities costs were according to published EIA pricing [5]: $4.01/MMBtu natural gas with 0.39% real escalation per year and $0.071/kWh electricity with -0.51% real escalation per year. Finance and tax assumptions included 100% equity financing, 10% real rate of return on equity, 26% investment tax credit, accelerated depreciation (5 years), and reduced property taxes.

Table 12. Characteristics of the TEA model hydrogen plant.

Parameters	Value
Production Scale, kg/day	100,000
Number of SMR units needed	
Solar only	11,400
Solar-electric hybrid	3,133
SMR pressure, bar	2
WGS stages	2
Reactor approach to equilibrium	
SMR	90%
WGS	90%
Syngas compression	
Final pressure, bar	13.5 (before PSA)
First stage compression	distributed
Second stage compression	central
Hydrogen separation	
PSA	central
Hydrogen recovery	90%

The TEA results and hydrogen cost projections are summarized in Table 13. Compared to conventional SMR, higher methane conversion and PSA H_2 recovery were more important for solar and solar-electric hydrogen plants because there was less use for PSA tail gas energy than in a conventional plant. The solar-only hydrogen plants were found to be more capital intensive than solar-electric hydrogen plants, but this was partly offset by the expense of electricity compared to solar energy for the hybrid plants. The net effect was a lower levelized cost per kg-H_2 for the hybrid plants. Hydrogen production costs for the solar-electric hybrid SMR were moderately higher than for hydrogen plants using only natural gas, but the hybrid plant had a reduced carbon footprint from the use of renewable energy.

The best economics were with chemical production applications because the syngas created had value beyond just its energy content. Both solar-only and solar-electric hybrid SMRs were projected to be able to achieve <$2/kg leveraged hydrogen production costs.

Table 13. Cost projections of solar and solar-electric hydrogen production plants.

	Solar Only	Solar-Electric
Hydrogen, kg/day	100,000	100,000
Initial Cost, $M	355	113
Levelized Costs		
Total, $/kg	1.81	1.55
Capital, $/kg	1.05	0.37
O&M, $/kg	0.16	0.08
Energy, $/kg	0.60	1.10

2.3.4   WBS 4.0 Palm Desert Demonstration

This task supported the effort towards the installation and testing of a demonstration Dish-STARS™ system for the production of hydrogen or the co-production of hydrogen and methanol. The lead for this task was STC with PNNL providing technical assistance. The task title referenced Palm Desert, CA, a potential demonstration site identified during project planning stage, not the actual site to be finalized by work under this project and any follow-on work. The technology and target application to be demonstrated were determined by STC based on the best choice to aggressively commercialize the Dish-STARS™ technology. The selected near-term demonstration target was hydrogen production at fuel cell electric vehicle (FCEV) filling stations in California.

The commercial demonstration target aimed for a potentially sizeable market as FCEVs are entering the marketplace at an accelerated pace. Cumulative sales or leases of FCEVs in California were 8,486 as of the third quarter of 2020. According to a survey of auto manufacturers by CARB, the number of FCEVs in California was estimated to grow to 27,000 by 2023 and 48,900 by 2026 [6]. In 2020, California had 45 open retail hydrogen refueling stations capable of serving nearly 20,000 light-duty FCEVs. It was estimated that the state would reach the goal of achieving over 100 publicly available stations, serving 150,000 light-duty FCEVs, by 2024 [7].

The team led by STC had evaluated market landscape and policy considerations to identify nearest-term opportunities for hydrogen generators. Many transit agencies – including multiple city opportunities in California and the Pacific northwest are potential users of low-cost hydrogen production systems. In long haul trucking industry, there are partnerships for joint development of fuel cell vehicles, e.g., Kenworth/Toyota and Nikola/GM, that will need hydrogen fuel to operate. Opportunities in federal and commercial fleet vehicles includes the transition of ~645,000 federal vehicles to Zero-Emission Vehicles (ZEVs), per January 27, 2021, Executive Order of the President. Incentives tied to California Low-Carbon Fuel Standards provide up to $2-3/kg Carbon Credits for the hydrogen used in FCEVs. Similar law is being considered Washington state legislature and the draft bill has been passed by the House. Washington Renewable Hydrogen Bills – State Law (SB5588), passed in 2019, and SB5000 (currently in consideration with bi-partisan support at time of this report), are additional policy examples that shape the market opportunities. Other opportunities surveyed by this team include distributed chemical processing,

such as processing farm waste, ammonia/fertilizer production, atmospheric CO_2 capture, utilization, and sequestration.

Cost of hydrogen has been limiting FCEV adoption and the deployment of filling stations. Distributed production of low-cost, low-carbon hydrogen based on STARS technology platform will enable FCEVs to compete in the marketplace. A conceptual illustration of this application, i.e., converting renewable natural gas to hydrogen in close proximity to the station using STARS hardware, in shown in Figure 30. At the end of the current project, the team continued work towards defining a follow-on project for a commercial demonstration in California with participants including SoCalGas, STC, Linde, Xebec, and Barr Engineering, as well as STC's numerous partners in STARS supply chain developed during this project, the RAPID project, and under STC's own development.
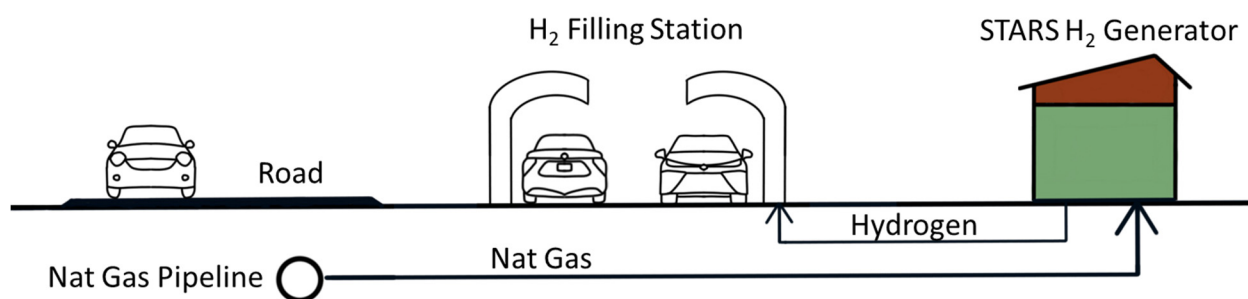

Figure 30. Conceptual illustration of low-cost hydrogen production for FCEV filling stations using STARS technology hardware.

The conceptual design developed under the current project was adapted to the specific near-term demonstration requirements selected by STC team. The earlier MPV designs were scaled and adapted to a new "Half-Hex" platform for hydrogen filling stations. It included three SMR reactors, one common WGS reactor, and balance of the plant components and was designed to produce 100 kg-H_2/day. The process heat was supplied by electrical induction coupled directly to the SMR reactors based on STC near-term commercial development plan. This platform can be viewed as the electric SMR section of the FEL-1 conceptual design detailed earlier in this report.

The team collaborated with the concurrent RAPID project to develop the design and manufacturing method of the SMR reactor units. It should be noted that such SMR reactor units are applicable for using either concentrated solar heat or electrical induction heat. Figure 31 shows one of the initial prototype STARS reactor units built in collaboration with the RAPID project by additive manufacturing methods. A CAD model of the Half-Hex piping layout is shown in Figure 32. The layout allows two Half-Hex units to be installed close together to double capacity with efficient use of space. Detailed engineering design including the balance of plant and control system had been initiated by STC and its partners. At the conclusion of this project, Half-Hex detailed design was about 85% complete with system assembly of the test prototype already initiated (Figure 33).

Figure 31. Photograph of one of the additively manufactured STARS reactor units built for the Half-Hex demonstration platform.
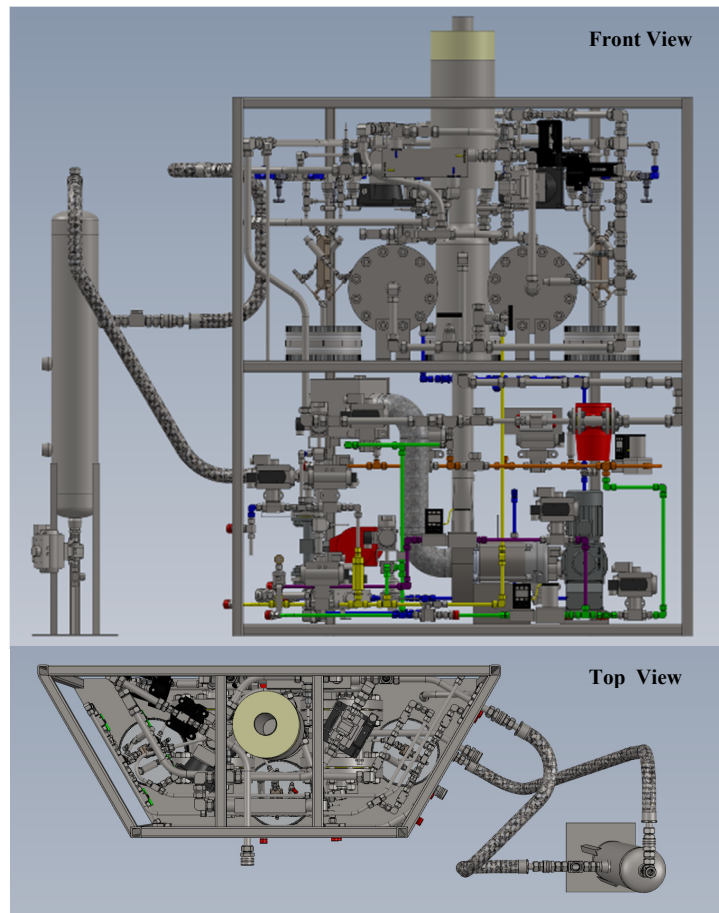

Figure 32. CAD models of the piping layout of the STARS Half-Hex platform for hydrogen production demonstration for FCEV filling stations (1, front view; 2, top view).

Figure 33. Half-Hex component fabrication and assembly photos (left, front side; middle, back side; right, vapor liquid separator).

The commercial demonstration set in motion by the current project culminated greater than $50M in government-industry funded research over 20 years in micro- and meso-channel process technology (MMPT) as showcased by Figure 34. There are opportunities for extended demonstration beyond the current project. Additional opportunities to improve solar thermo-economics further include component development for solar-thermal steam generation and solar-thermal enhancement to pressure swing adsorption for hydrogen purification. Dish solar-electric hybrid STARS system for around-the-clock operation will also be very attractive because of both better capacity factor and high-value use of excess renewable electricity when available from the grid. The STARS platform can play a crucial role of "chemical transformer" to enable an early on-ramp to a hydrogen grid, a connecting block for electricity-hydrogen-electricity with use of fuel cells, and the ability to add solar boost to energy content.
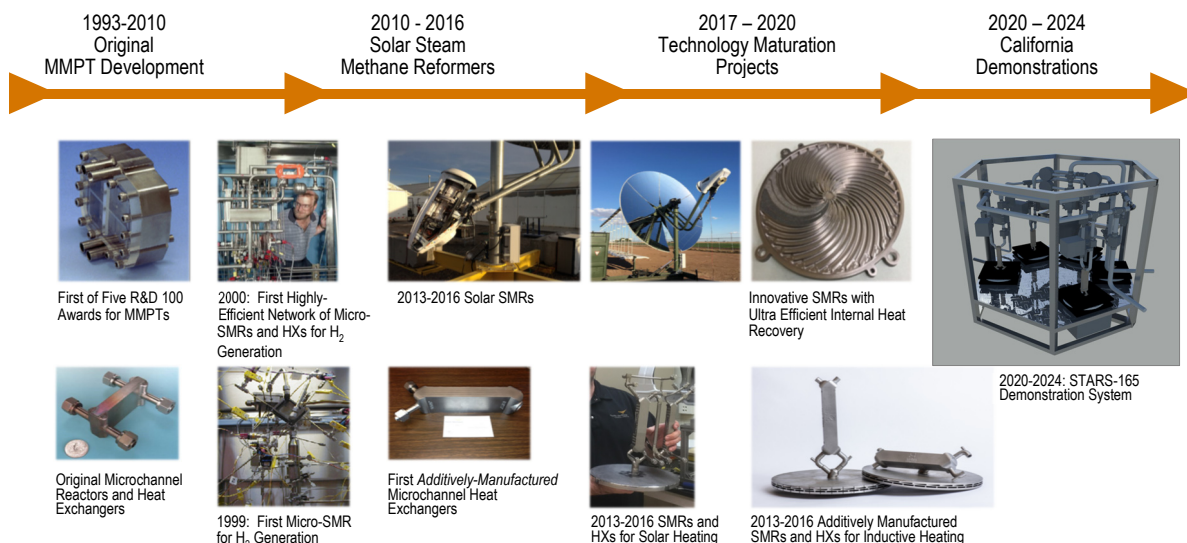

Figure 34. Legacy and evolution of MMPT technology for hydrogen generation at PNNL leading up to the planned STARS commercial demonstration.

3.0   Issues, Risks, and Mitigation

The project period of performance overlapped the COVID-19 global pandemic. The planned field operation at Brawley, CA, during 2019 and 2020 for on-sun testing of the TRL 7 reactor system had been severely curtailed. The original target of 300 hour extended testing was truncated to >100 hour testing. Towards the end of the project, the team obtained special DOE approval and traveled to the Brawley site to close out the testing facility.

4.0   Project Output

4.1   Awards

PNNL was a winner of the 2018 Award for Excellence in Technology Transfer by the Federal Laboratory Consortium (FLC), for its effort in developing and transferring the Solar Thermochemical Advanced Reactor System (STARS) to the STARS Technology Corporation (STC). PNNL and STC partnered with SoCalGas to show how STARS can lower carbon emissions in natural gas applications. Rick Perry, the Secretary of Energy at the time of the Award, wrote, "This demonstrates an important example of moving technology from Laboratory to the market, one that offers important benefits for our Nation and its citizens."

4.2   Technology Showcases

The project team, i.e., SoCalGas, STC, and PNNL, showcased a Dish-STARS™ reactor system exhibit at California Air Resources Board's (CARB) 50th Anniversary Technology Symposium at University of California Riverside on May 17, 2018.

The project team hosted a Dish-STARS™ live on-sun demonstration at San Diego State University Center for Energy Sustainability in Brawley, California, during a SoCalGas Renewable Energy Technology Demonstration Day event on June 27, 2019.

STC on behalf of the project team exhibited the Dish-STARS™ reactor system at 2019 California Special Districts Association Annual Conference and Exhibitor Showcase in Anaheim, California on September 26, 2019.

PNNL, STC, and SoCalGas hosted a "Reddit Ask Me Anything" (AMA) session on renewable hydrogen topics including Dish-STARS technology and engaged online community in discussions celebrating Hydrogen and Fuel Cell Day, October 7, 2019.

STC on behalf of the project team exhibited the Dish-STARS™ reactor system at 2019 Fuel Cell Seminar and Expo in Long Beach, California on November 7, 2019.

4.3   Conferences

"Natural Gas to Liquid Fuel – A Modular Approach for Fracking Sites", National Tribal Energy Summit, Washington DC, May 3, 2017

"Dish-STARS™ Solar Thermochemical Production of Hydrogen", American Institute of Chemical Engineers 2019 Annual Meeting, Topic Conference for Concentrated Solar Energy for Power Generation and Chemical Processing, Orlando, Florida, November 12, 2019

5.0   References

[1] X.-M. Liu, G. Q. Lu, Z.-F. Yan and J. Beltramini, "Recent Advances in Catalysts for Methanol Synthesis via Hydrogenation of CO and CO2," *Ind. Eng. Chem. Res.,* vol. 42, no. 25, pp. 6518-6530, 2003.

[2] M. B. Fichtl, D. Schlereth, N. Jacobsen, I. Kasatkin, J. Schumann, M. Behrens, R. Schlögl and O. Hinrichsen, "Kinetics of deactivation on Cu/ZnO/Al2O3 methanol synthesis catalysts," *Applied Catalysis A: General,* vol. 502, pp. 262-270, 2015.

[3] M. Alam, Thesis: Kinetics and Deactivation in the Methanol Synthesis Reaction, Norwegian University of Science and Technology, 2011.

[4] I. Fisher, H. Woo and A. Bell, "Effects of zirconia promotion on the activity of Cu/SiO2 for methanol synthesis from CO/H2 and CO2/H2," *Catalysis Letters,* vol. 44, pp. 11-17, 1997.

[5] "Annual Energy Outlook," EIA, 2021.

[6] "2020 Annual Evaluation of Fuel Cell Electric Vehicle Deployment," California Air Resources Board, 2020.

[7] Baronas, Jean; Achtelik, Gerhard, "Joint Agency Staff Report on Assembly Bill 8: 2020 Annual Assessment of Time and Cost Needed to Attain 100 Hydrogen Refueling Stations in California," California Energy Commission and California Air Resources Board, 2020.

Pacific Northwest
NATIONAL LABORATORY

Proudly Operated by **Battelle** *Since 1965*

902 Battelle Boulevard
P.O. Box 999
Richland, WA 99352
1-888-375-PNNL (7665)

www.pnnl.gov

U.S. DEPARTMENT OF
ENERGY